**ORIGINAL ARTICLE**

# Calcium channel blockade with nimodipine reverses MRI evidence of cerebral oedema following acute hypoxia

**Abbreviated Title:** Calcium channel blockade in cerebral hypoxia

Matthew J Rowland DPhil[1,2], Martyn Ezra FRCA[1,2], Anderson Winkler MD[1], Payashi Garry FRCA[1,2], Catherine Lamb[2], Michael Kelly PhD[1], Thomas W Okell DPhil[1], Jon Westbrook FRCA[1,2], Richard G Wise PhD[3], Gwenaëlle Douaud PhD[1], Kyle T Pattinson DPhil[1,2]

[1]Nuffield Department of Clinical Neurosciences, University of Oxford, Oxford OX3 9DU, UK

[2]Neurosciences Intensive Care Unit, Oxford University Hospitals NHS Trust, Oxford OX3 9DU, UK

[3]Cardiff University Brain Research Imaging Centre, School of Psychology, Cardiff, CF10 3AT, UK

**Corresponding author:**

Dr Matthew James Rowland, Nuffield Department of Clinical Neurosciences

6th Floor West Wing, John Radcliffe Hospital, Oxford OX3 9DU

matthew.rowland@ndcn.ox.ac.uk

Twitter: @matthewjrowland

+44 (0)1865 223 058

This research was supported by the JABBS Foundation and the National Institute for Health Research of Oxford Biomedical Research Centre based at Oxford University Hospitals NHS Trust and University of Oxford. MR and KP were supported by the Medical Research Council, UK: M.R. through a Clinical Research Training Fellowship (G100466) and K.P. through a Clinician Scientist Fellowship (G0802826). G.D. is supported by the UK MRC (MR/K006673/1).

## ABSTRACT

Acute cerebral hypoxia causes rapid calcium shifts leading to neuronal damage and death. Calcium channel antagonists improve outcomes in some clinical conditions, but mechanisms remain unclear.

In 18 healthy participants we: (i) quantified with multiparametric MRI the effect of hypoxia on the thalamus, a region particularly sensitive to hypoxia, and on the whole brain in general; (ii) investigated how calcium channel antagonism with the drug nimodipine affects the brain response to hypoxia.

Hypoxia resulted in a significant decrease in apparent diffusion coefficient (ADC), a measure particularly sensitive to cell swelling, in a widespread network of regions across the brain, and the thalamus in particular. In hypoxia, nimodipine significantly increased ADC in the same brain regions, normalizing ADC towards normoxia baseline. There was positive correlation between blood nimodipine levels and ADC change. In the thalamus, there was a significant decrease in the amplitude of resting-state functional MRI (ALFF) and an apparent increase of grey matter volume in hypoxia, with the ALFF partially normalized towards normoxia baseline with nimodipine.

This study provides further evidence that the brain response to acute hypoxia is mediated by calcium, and importantly that manipulation of intracellular calcium flux following hypoxia may reduce cerebral cytotoxic oedema

## Key Words

ADC, Calcium, Hypoxia, MRI, Nimodipine

## INTRODUCTION

Many important cellular processes are mediated by calcium. The movement and storage of calcium in cells are subject to tight regulatory control, primarily through the action of voltage gated calcium channels (L-type channels).[1] In neurons, these calcium channels are the principal source for calcium entry and membrane depolarization after energy failure.[2,3] Drugs, such as nimodipine, that block these calcium channels may reduce calcium influx into neurons and play a key role in limiting neuronal cellular damage due to oxygen deprivation (cerebral hypoxia).[2]

Nimodipine is an L-type calcium channel blocker characterized by a highly selective action on cerebral blood vessels and a high affinity for receptors in the brain.[4,5] This preferential cerebral action of the drug has been explained by high transfer across the blood-brain barrier compared with other calcium channel blockers.[6] Nimodipine has been shown to improve outcomes after brain haemorrhage, but this effect does not extend to other types of acute brain injury such as trauma and stroke where there is restriction in blood supply (ischaemia).[7] The precise mechanisms behind this beneficial effect remain unclear, but is likely to be related to blocking calcium influx after tissue ischaemia at a neuronal level.[8]

In both focal and global cerebral ischaemia, there is substantial evidence of variability in the tolerance of different brain regions to hypoxic-ischaemic damage. Sub-cortical structures including the thalamus, the hypothalamus, basal ganglia and cerebellum are particularly sensitive to hypoxic-ischaemic injury,[9-11] with the thalamus in particular showing early vulnerability in the acute phase.[12] Poor functional recovery, (specifically in memory) has also been linked to damage in the thalamus in animal studies,[13] as well as cognitive dysfunction in patients surviving cardiac arrest and traumatic brain injury.[14,15] The thalamus is therefore a particularly interesting brain structure in which to investigate the

role of calcium in mediating cerebral injury following hypoxia, especially as thalamic voltage dependent calcium channels are likely to play a key role in higher-level cortical functions.[16]

Exposure of healthy volunteers to experimental hypoxia potentially offers a model of *in vivo* reversible brain injury. Heterogeneous changes in diffusion weighted imaging metrics (e.g. apparent diffusion coefficient (ADC) – an MRI marker of cerebral oedema), cerebral blood flow (CBF) and cerebral volume have all been previously reported after acute hypoxia.[17-19] There has also been recent interest in the significance of the amplitude of low frequency oscillations (ALFF) (0.01 to 0.1Hz) of resting state functional MRI in health and in disease. Changes in ALFF have been observed following traumatic brain injury[20] and in Parkinson's disease.[21] Low frequency oscillations in calcium (known as a biomarker of cellular oscillations) show frequencies similar to those of deoxyhemoglobin (the main contributor to the BOLD MRI signal) and precede them by 5–6s.[22] Changes in ALFF due to cellular calcium flux might therefore represent a biomarker of acute cerebral tissue hypoxia and be influenced by calcium channel blockade with nimodipine.

The purpose of this study was two-fold: first, to test the hypothesis that acute hypoxia would have a significant effect on the thalamus, and second, that this hypoxic effect would be attenuated by the administration of nimodipine. To test these hypotheses, the objectives of this study was to quantify changes in ADC, grey matter volume, cerebral blood flow and ALFF associated with acute hypoxia using MRI in healthy humans. We then aimed to investigate the impact of calcium channel blockade with nimodipine on these changes, to offer mechanistic insights into therapeutic calcium channel blockade clinically in patients.

## MATERIALS AND METHODS

The study was conducted in accordance with the Helsinki Declaration as revised in 2008 and was approved by the local UK National Research Ethics Service Committee (NRES Committee South Central – Berkshire: 11/SC/0519). Informed written consent was obtained from all participants. 20 right handed, healthy volunteers (11 males and 9 females, mean age 28 ± 8 years) with no regular medication were recruited. Specific exclusion criteria included routine contraindications to MRI scanning, history of smoking and recent air travel or exposure to high altitude within the last month.

### Experimental Design

Participants attended four separate experimental sessions (a minimum of one week apart). Each session lasted approximately five hours in total. The experiment was a factorial design with the order of each session randomised for each subject. The experimental conditions are shown in Figure 1A and were as follows:

1. Poikilocapnic normoxia ("normoxia")/Placebo
2. Poikilocapnic normoxia ("normoxia")/Nimodipine
3. Poikilocapnic hypoxia ("hypoxia")/Placebo
4. Poikilocapnic hypoxia ("hypoxia")/Nimodipine

All conditions were normobaric. Drug/placebo conditions were double blinded for each session with doses prepared by an individual independent of the research group. Participants were blinded to gas mixture in all sessions. The researchers running each experimental session were not blinded to the gas mixture. First level MRI analysis was undertaken blinded to both normoxia/hypoxia and drug/placebo conditions. Un-blinding

was only performed once all first level MRI pre-processing and analysis had been completed.

**Experimental Procedure**

The study protocol consisted of a continuous four hour session in a physiology laboratory breathing either room air, with the usual fraction of inspired oxygen ($FiO_2$) of 21%, or a hypoxic gas mixture with the partial pressure of end-tidal oxygen ($P_{ET}O_2$) maintained at 7.3KPa, followed by an MRI scan with $P_{ET}O_2$ maintained at the same level as during the preceding four hours. Depending on the session protocol (as per Figure 1A), participants received either nimodipine 30mg or placebo at both one hour and three hours into the protocol depending on the experimental condition.

**Acute hypoxia**

Modulation of inspired $O_2$ content during both the laboratory and MRI sessions was achieved using a custom-built breathing apparatus (Figure 1B). During the laboratory hypoxia condition, subjects inhaled gas from a hypoxicator unit (HYP-123 Hypoxicator generator, Hypoxico Inc) with an FiO2 of 12% (equivalent to an altitude of 4400m) via a tight-fitting silicone facemask (Hans Rudolph, 7540 series V2, Kansas City, MO, USA) to maintain an $P_{ET}O_2$ of 7.3KPa. Additional 7% $O_2$ in nitrogen from a cylinder was added as required to ensure tight control of $P_{ET}O_2$ for each participant. During the normoxia condition, subjects received medical air at the same rate through the same system.

The partial pressure of end-tidal carbon dioxide ($P_{ET}CO_2$) was not experimentally controlled during the laboratory and MRI sessions to replicate normal cerebral physiological responses to hypoxia. Continuous physiologic recordings were obtained for $P_{ET}CO_2$ and $P_{ET}O_2$ (Gas Analyzer, AD Instruments, UK). Oxygen saturations ($SpO_2$),

heart rate and non-invasive blood pressure (NIBP) were measured every five minutes (Dinamap Procare 300, GE Healthcare). For each subject, the hypoxicator was turned on during all four sessions to ensure the background noise was the same and that subjects remained blinded to the gas mixture condition. During the MRI session, participants used a similar breathing apparatus and a diving mouth-piece (Scubapro Ltd, UK) to maintain the same $P_{ET}O_2$ as used in the laboratory session for the duration of the MRI scan.

**Study drug**

Nimodipine and placebo doses were produced by Ipswich NHS Pharmacy Manufacturing Unit. Capsules were matched in colour, size and shape to ensure both participants and investigators remained blinded to the experimental condition. The dosing and oral route were chosen to replicate standard clinical practice in patients with subarachnoid haemorrhage and timed to aim for maximum serum concentrations of the drug at the start of the MRI scanning session (based on data from Hernández-Hernández R. et al[23]). Although it was difficult to ensure peak concentrations of nimodipine at the same timepoint in each session, blood samples were taken from each participant at the 4 hours mark in each session and any delay between blood sampling and MRI scanning was the same for each session. Serum nimodipine levels were then measured using customised mass spectroscopy (Sequani Ltd).

**MRI Scanning**

A Siemens MAGNETOM 3T Verio scanner (Siemens Healthcare, Erlangen, Germany) situated immediately adjacent to the physiology laboratory was used for all scanning sessions. At the end of the four-hour laboratory session, participants were moved immediately to the scanner room and placed directly onto the breathing system. Disconnection time was kept to an absolute minimum. Heart rate, oxygen saturations

($SpO_2$) and non-invasive blood pressure (NIBP) were continuously monitored during MRI scans using an MRI-compatible physiological monitoring system (3150/3155 MRI patient monitor, In Vivo Research). Tidal $O_2$ and $CO_2$ were monitored using a gas analyzer (Gas Analyzer, AD Instruments, NZ).

The scanning protocol included:

- **T1-weighted MPRAGE structural, to measure changes in grey matter (GM) volume**: 2 mins 22 s, whole brain; 1.5 x 1.5 x 1.5mm resolution; TR 1780 ms; TI 900 ms; TE 4.4 ms
- **Diffusion-weighted (DWI) echo planar, spin echo sequence, to measure changes in ADC**: 1 min; TR 5300 ms; TE 91 ms; b values 0 and 1000 s/mm$^2$, voxel size 1.8 x 1.8 x 5mm; 25 slices, isotropic encoding
- **Time-of-flight MR neck angiogram, to facilitate vessel labeling**:1.5 mins; 20 slices; 1.2 x 0.8 x .1.3 mm; TR 26 ms; TE 3.43 ms; flip angle 18 degrees
- **Multi-inversion time (TI), vessel-encoded pseudo-continuous arterial spin labeling (VEPCASL) perfusion-weighted imaging, to measure changes in CBF** (as per Okell et al., 2013[24]): 5 mins 55 s, 3.4 x 3.4 x 4.5 mm, field of view 220mm; TR 4080 ms; TE 14 ms, echo planar imaging readout, 24 slices, background suppression with multiple post-labeling delays (tag duration 1.4 s with six delays: 0.25 s, 0.5 s, 0.75 s, 1 s, 1.25 s, 1.5 s) along with calibration scans acquired with both head and body coils for signal reception (24 s each, TR 6000 ms)
- **Phase contrast scan, to quantify flow velocities through carotid/vertebral vessels**: 1 min 27 s, 1.9 x 1.9 x 5mm, TR 58.75 ms, TE 6.06 ms, flip angle 15 degrees, VENC 100cm/s

- **Resting state gradient-echo, echo-planar blood oxygen dependent level (BOLD) imaging sequence - to measure low frequency fluctuations in the BOLD signal**: 6 mins; TR 3000 ms; TE 40 ms; flip angle 90°; FOV 240 mm; voxel size 3.0 x 3.0 x 3.0 mm, 40 slices
- **B0 fieldmap images –** to aid registration by correcting for echo-planar imaging distortion artifacts

The scanning protocol was ordered as presented above and was conducted in the same order for each experimental session. To quantify any potential change in velocity through the carotid and vertebral arteries due to either hypoxia or nimodipine, phase contrast images were acquired. This technique utilizes the phase of an image to encode the velocity of flowing spins and has been validated for angiogram and quantitative flow measurements.[25]

**Post-processing of MRI data**

All imaging analyses were carried out using FSL Version 5.0 (FMRIB Software Library, Functional Magnetic Resonance Imaging of the Brain Centre, Department of Clinical Neurosciences, University of Oxford, Oxford, UK, http://www.fmrib.ox.ac.uk[26]) unless otherwise specified.

Volumetric structural data analysis

An optimized voxel-based morphometry (VBM) analysis was undertaken on the T1-weighted images to identify regional changes in the thalamus and whole brain grey matter volume (FSL-VBM: http://fsl.fmrib.ox.ac.uk/fsl/fslwiki/FSLVBM[27]). All images were processed following the same protocol: first, structural images from all four experimental conditions, in all subjects, were brain-extracted and grey matter-segmented before being

registered to the MNI152 standard space using non-linear registration. The resulting images were averaged and flipped along the x-axis to create a left-right symmetric, study-specific grey matter template. Second, all native grey matter images were non-linearly registered to this study-specific template and "modulated" to correct for local expansion (or contraction) due to the non-linear component of the spatial transformation. The modulated grey matter images were then smoothed with an isotropic Gaussian kernel with a sigma of 3mm. A thresholded (at 35%) binarised probabilistic mask (Harvard-Oxford, FSL) of the thalamus in MNI152 standard space was used to obtain values for grey matter volume of both the thalami.

We also investigated voxel-wise changes in volume over the whole brain grey matter, using permutation-based non-parametric testing (5,000 permutations), correcting for multiple comparisons across space (see Statistical analysis section below for further details).

DWI data analysis

ADC maps obtained from the scanner were brain extracted using the FSL tool BET[28] and registration of the B0 image to the native T1-weighted image was estimated for each subject with boundary based recognition.[29-31] Next, we combined this within-subject registration with the non-linear registration of each subject's grey matter-segmented image to the VBM template. At the end of this registration process, ADC maps were therefore in the study-specific VBM template space to ensure optimal group registration. The same probabilistic mask of the thalamus used in the VBM analysis was applied to maps from each condition to obtain average values for each participant. Finally, voxel-wise statistical test was applied using permutation-based non-parametric testing to look for changes in grey matter ADC across the whole brain between the conditions of interest.

Perfusion-weighted data analysis

All related data processing steps essential for quantification of CBF including tissue segmentation, estimation of equilibrium magnetization of blood ($M_0$b) from the mean CSF (cerebrospinal fluid) magnetization ($M_0$csf) within a ventricle mask, and generation of absolute CBF in physiologic units (ml blood/100g tissue/minute) were completed using FSL tools and MATLAB (MATLAB R2015a, The MathWorks Inc., Natick, MA, 2000) as per Okell et al., 2013.[24]

Firstly, head motion was corrected using multi-resolution rigid body co-registration of volumes, as implemented by MCFLIRT. Then multi-TI VEPCASL data was processed using a non-linear fit to the general arterial spin labeling (ASL) kinetic model for all voxels within a whole brain mask, accounting for macrovascular signal, to quantify CBF.[24,32] Similarly to the ADC analysis, total perfusion maps were registered to the study-specific VBM template space by combining the spatial transformation of each calibration body EPI image to the same subject's T1-weighted image with the corresponding VBM warpfield. Again, the probabilistic mask of the thalamus was used to obtain average values for thalamic CBF.

Phase contrast MRI was used to assess the blood velocity in the carotid and vertebral arteries at the location of the PCASL labelling plane.[25] The phase contrast MRI acquisition was cardiac-gated using a pulse oximeter. Vessel ROIs were manually created and applied to the cardiac gated velocity maps to provide plots of blood velocity over the cardiac cycle. Average velocity was then computed and compared to a simulated plot of inversion efficiency versus velocity. Average vessel velocities in the range of 15 cm/s to 45 cm/s result in an inversion efficiency of approximately 0.9[33], and were in this range for all

subjects. As a result, the effects of blood velocity at the labelling plane on inversion efficiency were likely to be consistent across all subjects.

Amplitude of low frequency fluctuations analysis:

Head motion was corrected using multi-resolution rigid body co-registration of volumes, as implemented by MCFLIRT. Brain extraction was carried out for motion corrected BOLD volumes as implemented in BET. This procedure was verified with visual inspection of the extraction result for each data set acquired.

Data denoising was performed using an independent component analysis (ICA) approach which was used to decompose FMRI data into different spatial and temporal components using FSL's MELODIC (Multivariate Exploratory Linear Optimised Decomposition into Independent Components[34]). The noise components were manually identified based on spatial location of signal, time course and signal frequency.[35] The FSL tool FIX[36,37] was then used as follows:

1. To regress the full space of the motion confounds obtained from MCFLIRT from both the data and from all the ICA component time-series;
2. To estimate the contribution of both “signal” and “noise” components as a means of identifying the noise specific variance;
3. To remove the unique contribution of the components identified above as "noise" from the data.

Additional data denoising in 13 subjects was also performed using a combination of physiological noise modelling integrated in FEAT (RETROICOR[38,39]) and ICA (described in [40]) to assess the impact of measured changes in respiratory and heart rate on ALFF

between sessions. We were unable to perform this correction on all datasets as five subjects had intermittent short (5-10 seconds) interruptions in continuous physiological traces during scanning which rendered analysis with RETROICOR impossible, so these five subject were excluded from this supplementary analysis. Results and figures from this analysis are presented in the Supplementary Material.

We again registered the fMRI volumes to the VBM study-specific template space. The resulting images were smoothed with 6mm full width at half maximum (FWHM) Gaussian kernel.

Calculation of ALFF was then performed with customised MATLAB (Mathworks Inc.) scripts using the Chronux Toolbox (www.chronux.org). The power of the low frequency fluctuations in the frequency range 0.01-0.1Hz was measured using a multi-taper spectral estimation[41] using discrete prolate spheroidal (Slepian) sequences with five tapers, and fast Fourier transform algorithm for the resting-state time series for each voxel. The power between the 0.01-0.1Hz band was divided by the total power of the resolved frequencies from 0Hz to the Nyquist frequency to calculate normalised spectral power for that low frequency band. This was performed to look specifically at changes within this low power band. We used the same probabilistic mask of the thalamus to obtain average values for ALFF in the thalamus region.

**Statistical Analysis**

The contrasts of interest between conditions were:

1. Effect of hypoxia on brain: Normoxia/Placebo v Hypoxia/Placebo
2. Effect of nimodipine in normoxia: Normoxia/Placebo v Normoxia/Nimodipine
3. Effect of nimodipine in hypoxia: Hypoxia/Placebo v Hypoxia/Nimodipine

Statistical differences between these conditions were assessed using permutation tests,[42] with the FSL tool randomise for the voxelwise analyses, using 5,000 permutations, and with the tool PALM (Permutation Analysis of Linear Models (https://fsl.fmrib.ox.ac.uk/fsl/fslwiki/PALM) for the region-based analyses, using 10,000 permutations followed by the approximation of the tail of the permutation distribution using a generalized Pareto distribution.[43] Each p-value was adjusted for six comparisons, these being the three differences in the positive and negative directions. Significance for all tests was established at the level alpha<0.05. Finally, a repeated measures ANOVA was applied to the region-based data to investigate the presence of an interaction between drug conditions and oxygenation conditions to investigate whether nimodipine significantly modulates the response to hypoxia.

For the voxelwise analyses in each modality, to account for the repeated measures, the differences were calculated between each contrast (e.g. normoxia/placebo v hypoxia/placebo) and then entered into a one sample t-test, assessed with sign flippings. Voxelwise analyses used Threshold-Free Cluster Enhancement (TFCE)[44], with familywise error rate corrected across space. Results were considered significant at the level alpha<0.05.

The Pearson correlation coefficient was used to investigate correlations between blood levels of the drug nimodipine and MRI changes seen between the Hypoxia/Placebo and Hypoxia/Nimodipine conditions with results considered significant at $p < 0.05$.

## RESULTS

Complete laboratory and MRI datasets were obtained in 18 out of the 20 subjects. Two subjects withdrew from the study due to scheduling issues preventing completion of all

sessions. During pre-processing and prior to unblinding, significant motion artifact was discovered in one VEPCASL dataset throughout all sessions. This subject was therefore excluded leaving only 17 subjects for the VEPCASL group analysis.

**Physiological data**

Figure 2-A shows changes in mean $P_{ET}O_2$ and Figure 2-B shows changes in end tidal carbon dioxide ($P_{ET}CO_2$) levels throughout the laboratory and MRI sessions for all participants. The differences in $P_{ET}CO_2$, $P_{ET}O_2$, $SpO_2$, heart rate and non-invasive blood pressure between each condition are summarized in Table 1 along with significance values.

Compared with normoxia, as expected, the hypoxia condition significantly reduced the $P_{ET}O_2$ in both the placebo and nimodipine conditions. There was a drop in $P_{ET}CO_2$ values for both the placebo and nimodipine conditions with hypoxia as the laboratory and MRI sessions progressed.

Nimodipine had no significant effect on either $P_{ET}O_2$ or $P_{ET}CO_2$ compared to placebo in either the normoxia or hypoxia conditions. Hypoxia resulted in a significant drop in $SpO_2$ and increase in heart rate in both placebo and nimodipine conditions. There was no significant difference in mean arterial pressure between normoxia and hypoxia and with nimodipine.

**Nimodipine levels**

Serum nimodipine levels for each experimental condition are presented in the Table 1. Importantly, there was no significant difference in nimodipine levels between the normoxia and hypoxia sessions (18.90 ± 20.33 ng/ml v 24.07 ± 24.62 ng/ml, p=0.73).

**MRI Results**

Figure 3 shows the MRI results for the thalamus from the study for the DWI (Figure 3A), structural (Figure 3B) and perfusion-weighted images (Figure 3C). Figure 4 shows data from the voxelwise whole-brain comparisons for the DWI data. Figure 5 shows the results of the ALFF analysis. Figure 6 shows the correlations between nimodipine levels and change in MRI data for Hypoxia/Placebo and Hypoxia/Nimodipine conditions.

Tables S2 and S3 in the supplementary material show the common local peaks of the significant clusters for Figure 5.

Effect of acute hypoxia

*Diffusion-weighted imaging*

There was a significant decrease in ADC values in the thalamus for the hypoxia condition compared to the normoxia condition (1061 ± 40 v 1011 ± 75 x $10^{-6}$mm$^2$/s, p=0.0002)(Figure 3A). Whole brain voxelwise analysis confirmed regional variation in grey matter ADC associated with the hypoxia condition, with especially noticeable decreases in ADC seen in the subcortical structures (thalamus, basal ganglia, hippocampus) as well as the cerebellum (crus I and II regions – Figure 4A).

*T1-weighted imaging*

Figure 3B shows that hypoxia resulted in a significant apparent increase in grey matter volume in the thalamus ROI when compared to normoxia (0.3924 ± 0.028 v 0.370 ± 0.037 a.u., p=0.0027). Looking voxelwise over the whole brain though, there was no significant difference in grey matter volume.

*Perfusion-weighted imaging*

Figure 3C shows the results from the ASL perfusion-weighted imaging data for each experimental condition. There was an increase in CBF in the thalamus ROI for the hypoxia condition compared to normoxia (59.15 ± 10.00 v 50.34 ± 6.68 ml/100g/min, p=0.0191). However, looking at the whole brain grey matter voxelwise analysis, there were no areas of significant difference in grey matter CBF between the normoxia and hypoxia conditions.

Table 1 also presents the results for the phase contrast imaging for each experimental condition. Flow through both carotid arteries was significantly higher in the normoxia condition when compared to hypoxia. This was not the case for the vertebral arteries, where there was no significant difference in flow values.

*Amplitude of low frequency fluctuations*

There was a large increase in normalised ALFF in the thalamus (35.24 ± 2.43 v 41.20 ± 1.85, p=<0.0001) with hypoxia compared to normoxia (Figure 5). Results for grey matter are provided for comparison along with full power spectra for both the thalamus ROI and whole brain grey matter. These differences remained significant when the additional data physiological denoising was conducted as described in the materials and methods section (See Supplementary Data).

Effect of nimodipine under conditions of normoxia

*Diffusion-Weighted Imaging*

There was no significant difference between nimodipine and placebo in the thalamus (1061 ± 40 v 1050 ± 55 x $10^{-6}$$mm^2$/s, p=0.1363). There was also no significant regional or global effect on whole brain grey matter ADC values using voxelwise analysis.

*T1-weighted imaging*

Like the DWI data, compared with placebo, there was no significant difference in volume in the nimodipine condition for the thalamus (0.370 ± 0.037 v 0.3781 ± 0.035 a.u., p=0.2370) and no significant difference seen over whole brain grey matter using voxelwise analysis.

*Perfusion-weighed imaging*

There was a significantly increased thalamic CBF in the nimodipine condition compared with placebo (59.49 ± 11.70 ml/100g/min v 52.26 ± 6.91 ml/100g/min, p=0.037). However, there was no significant difference seen over whole brain grey matter using voxelwise analysis. Looking at the phase contrast results, velocities through carotid and vertebral arteries were not significantly different between the nimodipine and placebo conditions.

*Amplitude of low frequency fluctuations*

There was a significant reduction in normalised ALFF in the thalamus between nimodipine and placebo in the normoxia condition (41.20 ± 1.85 v 40.24 ± 1.88, p=0.028). Again, full power spectra and values for grey matter are provided for comparison in Figure 5.

Effect of nimodipine under conditions of hypoxia

*Diffusion-Weighted Imaging*

In the hypoxia condition, there was a significant increase in ADC values with nimodipine towards baseline in the thalamus compared to placebo (1059 ± 49 v 1048 ± 34 x $10^{-6}$$mm^2$/s, p=0.0171). There was also a significant interaction effect between nimodipine and hypoxia (p=0.0002). Furthermore, there was also a significant positive correlation between the change in ADC values in the thalamus between hypoxia/placebo and hypoxia/drug conditions and serum nimodipine levels (r=0.60 p=0.0083) with higher nimodipine levels in subjects associated with greater change in ADC values (Figure 6).

Figure 4B shows the voxelwise changes between the hypoxia/placebo and hypoxia/nimodipine conditions. Again, there was a significant increase in ADC across multiple subcortical regions including the thalamus, basal ganglia (putamen and caudate), hippocampus and cerebellum with the administration of nimodipine.

Finally, voxelwise comparison was performed between normoxia/placebo and hypoxia/nimodipine which showed no significant differences over whole brain grey matter confirming the reversal of the effect of acute hypoxia.

*T1-weighted imaging*

Nimodipine had no significant effect on the volume of the thalamus (0.382 ± 0.050 v 0.392 ± 0.028 a.u., p=0.5291) in hypoxia versus placebo. There was no significant interaction effect either between drug condition and oxygenation condition (p=0.1480). Voxelwise analysis showed no significant effect on whole brain grey matter volumes.

Finally, there was no significant correlation between the change in the thalamus volume between hypoxia/placebo and hypoxia/drug conditions and serum nimodipine levels (r=-0.04, p=0.87).

*Perfusion-weighted ASL imaging*

We did not observe any significant difference in the thalamus CBF under conditions of hypoxia for nimodipine versus placebo (60.29 ± 12.00 v 58.48 ± 7.86 ml/100g/min, p=0.9158) or any voxelwise differences in grey matter CBF. There was also no significant interaction effect (p=0.4042). There was also no significant correlation between the change in the thalamus CBF between hypoxia/placebo and hypoxia/drug conditions and serum nimodipine levels (r=-0.188 p=0.4710).

Looking at the phase contrast results, velocities through both carotid and vertebral arteries were not significantly different between the nimodipine and placebo conditions under conditions of hypoxia.

*Amplitude of low frequency fluctuations*

In the thalamus, there was a significant increase in ALFF with nimodipine when compared to placebo (37.87 ± 1.66 v 35.24 ± 2.43, p=0.0003)(Figure 5). Furthermore, there was a significant interaction effect between drug and oxygenation conditions (p=0.0002). Like the DWI results, the degree of increase in thalamic ALFF with nimodipine in hypoxia showed a significant positive correlation with nimodipine levels (r=0.54, p=0.02).

## DISCUSSION

The aim of this study was to test the hypothesis that calcium channel activity mediates the cerebral response to inspiratory hypoxia *in vivo* in humans. Through this, we aimed to clarify the role of calcium in the pathophysiology of acute brain injury in clinical practice. Several notable findings have arisen from this study. Firstly, acute hypoxia causes a clear reduction in ADC and ALFF values in the thalamus. These changes are accompanied by an apparent increase in thalamic volume, together with an increase in thalamic CBF. Calcium channel blockade with nimodipine attenuated the effects of cerebral hypoxia on ADC and ALFF values seen in the thalamus and other cortical/sub-cortical areas, returning values back towards baseline levels seen in normoxia. Finally, changes in ADC and ALFF with nimodipine showed a significant correlation with nimodipine levels in hypoxia.

### Cerebral effects of acute hypoxia

Previous studies using MRI to investigate the effect of acute hypoxia on the brain have reported contradictory results showing either increased[17,19] or reduced[18,45,46] ADC values.

This may be due to differences in study/MRI protocols, duration of hypoxic stimulus and barometric pressures. In our study, the duration of hypoxia was chosen at four hours in order to compensate for initial changes in cerebral blood flow and ventilation that occur in the first 30 minutes post-hypoxic stimulus[47] and to allow potential MRI biomarkers of pathophysiological changes associated with hypoxia to develop. Our results demonstrate that the thalamus is sensitive to acute inspiratory hypoxia with significantly decreased ADC values. These results were replicated in a secondary voxelwise whole brain analysis. This further highlighted decreased ADC in other subcortical structures such as the caudate, putamen, hippocampus and cerebellum – areas also known to be susceptible to hypoxic-ischaemic damage. Reduced ADC values are generally interpreted to be due to cytotoxic oedema associated with intracellular swelling, and are associated with changes in cellular energy status responsible for reduced Na+/K+ ATPase pump and altered ionic homeostasis.[17,19]

Analysis of the T1-weighted data shows that thalamic volume was apparently increased with acute hypoxia. Other studies have reported similar effects following exposure to acute hypoxia with increased total brain and grey matter volumes associated with reduced whole brain ADC.[18,45] This increase is likely to result from cellular swelling due to cerebral oedema associated with inspiratory hypoxia. MRI evidence of cerebral oedema has also been noted as early as the first hour of hypoxic exposure, associated with significant shifts in intracranial CSF volumes.[48]

The results from the VEPCASL analysis suggest this increase may be due to the increase in CBF seen with acute hypoxia on CBF in the thalamus. Voxelwise changes in CBF were not seen over the whole-brain which is in concordance with other studies which have reported no difference in whole brain grey matter CBF in acute poikilopcapnic hypoxia.[45]. It

may also reflect the cerebral vasoconstriction that occurs because of the increased ventilatory response to hypoxia as well as issues with signal-to-noise ratio seen with ASL studies.

**Effects of calcium channel blockade on cerebral physiology during normoxia.**

In normoxia, nimodipine had no significant effect on ADC nor grey matter volume in the thalamus. However, there was a significant 14% increase in thalamic CBF and a reduction in ALFF. Nimodipine is characterized by a highly selective action on cerebral blood vessels and a high affinity to receptors in the cerebral cortex - hence the interest in its use clinically following acute brain injury. However, the literature investigating the effect of nimodipine on CBF is inconsistent. Early studies in animals under conditions of ischaemia demonstrated no effect on cerebral metabolism but increases in CBF due to a direct vasodilatory effect across all brain regions, particularly following disruption of the blood-brain barrier.[4,49-51] However, nimodipine had no significant effect on normal CBF or metabolism in animals.[52] Early studies into nimodipine in both healthy volunteers and patients suffering from stroke suggested a small overall increase in CBF after nimodipine treatment, with a redistribution of blood to hypoperfused regions in patients.[53,54] However, subsequent studies have shown no effect of nimodipine in healthy volunteers in concordance with the results of our study. [55] This may be as a result of differences in drug dose and timing as well as differences in CBF measurement techniques.

**The effect of nimodipine under conditions of cerebral hypoxia**

Results from this study demonstrate that nimodipine reverses decreases in both ADC and ALFF seen in the thalamus with acute hypoxia without an apparent effect on CBF The whole brain analysis also showed similar increases in ADC across the GM including subcortical structures such as the putamen, caudate, hippocampus and cerebellum. There

was also a significant positive correlation between the change in ADC values between Hypoxia/Placebo and Hypoxia/Nimodipine conditions and serum nimodipine levels in the thalamus. Voltage-gated calcium channels are essential for calcium signaling in excitable cells and play a key role in the final common pathway of acute cerebral ischaemia. Furthermore, L-type channels are known to display a particularly high sensitivity to hypoxia.[56] In experimental models of focal and global ischemia, L-type calcium channel antagonism with nimodipine has been shown to have a neuroprotective effect, attenuating cognitive dysfunction and increasing the hypoxic tolerance of brain tissue.[57,58] Nimodipine has also consistently been shown to reduce the incidence of secondary cerebral ischaemia and improve clinical outcomes after aneurysmal subarachnoid haemorrhage[59-61] – without any effect on cerebral vasodilatation.

Our results suggest that calcium channel blockade with nimodipine acts to reduce cytotoxic cerebral oedema following acute cerebral hypoxia without increased CBF. Other studies have suggested that nimodipine may have an effect on cerebral metabolism[62] which may underlie this effect on ADC and explain the clinical benefit seen in SAH, a condition characterized by high levels of cytotoxic cerebral oedema. Finally, there did not appear to be a difference in $P_{ET}CO_2$ with nimodipine, suggesting that changes in CBF are unlikely to be due to differences in ventilatory control. Other studies have demonstrated that nimodipine does not seem to exert a significant impact on the effect of hyperventilation in reducing regional CBF[63] and interferes with the CBF response to alterations in arterial CO2.[64] This may partially explain why there was no significant increase in CBF with nimodipine under conditions of hypoxia.

The variation in nimodipine levels despite consistent dosing between subjects suggests that the pharmacodynamics of the oral administration route may be an important factor in

the use of nimodipine clinically in patients. There was also a strong correlation between serum nimodipine levels and changes in ADC and ALFF seen with nimodipine in hypoxia. This highlights that monitoring of drug levels may be important if consistent clinical outcome benefits are to be achieved e.g. following subarachnoid haemorrhage.

**Amplitude of low frequency oscillations**

To date, no other studies have considered the exact role of the ALFF in cerebral hypoxia. Clinical studies have suggested that changes in ALFF in disease states may be a marker of brain damage. Altered ALFF in frontal brain regions is seen in patients recovering from traumatic brain injury[20], as well as in the cerebellum in patients with migraine and depression.[65,66] Increased ALFF in the thalamus is also positively correlated with microstructural damage seen on MRI in multiple sclerosis.[67] Our results show that acute inspiratory hypoxia results in a significant drop in thalamic ALFF in the BOLD signal replicating changes seen in disease states. Calcium channel blockade with nimodipine in normoxia also leads to a significant decrease in ALFF in the thalamus – potentially due to the role of calcium oscillations in resting brain neuronal activity. However, in the presence of hypoxia, the administration of nimodipine significantly increases ALFF normalizing levels to those seen in normoxia. Regional heterogeneity in the BOLD response to hypoxia has previously been reported in both animal studies[68,69] and studies in humans.[70] The underlying mechanisms that could lead to this are poorly understood and include different changes in total deoxyhaemoglobin for a fixed change in arterial oxygen saturation due to different blood volumes and/or different oxygen extraction fractions and flow-induced variation in saturation and signal intensity.[69] It may be that subcortical structures such as the thalamus have a different oxygen extraction fraction at rest than other areas of the brain and are therefore more sensitive to changes in arterial oxygen content. Though the absence of significant correlation between CBF and change in ALFF with nimodipine in

hypoxia suggests that this difference may be related to a mechanism of action of calcium channel blockade on neurons (potentially via an effect on low frequency oscillations in calcium levels) rather than a direct vascular effect.

## CONCLUSION

In summary, we have provided evidence for a preferential effect of calcium channel blockade with nimodipine under conditions of acute cerebral hypoxia in reversing changes in ADC and ALFF in the thalamus. These changes to ADC and ALFF may underlie the benefit seen clinically in conditions like SAH where significant global cytotoxic cerebral oedema is seen with early brain injury. Further research is needed into the importance of changes in ALFF with hypoxia and whether this represents a biomarker of cerebral tissue hypoxia in acute acquired brain injury.

## ACKNOWLEDGEMENTS

The authors would like to thank the Oxford Acute Vascular Imaging Centre and the Oxford University Clinical Academic Graduate School for their support.

## AUTHOR CONTRIBUTIONS

**Matthew J Rowland:** Study design, data acquisition, data analysis, interpretation of data, manuscript preparation, final approval

**Martyn Ezra:** Data analysis, interpretation of data, manuscript preparation, final approval

**Anderson Winkler:** Interpretation of data, critical revision of manuscript, final approval

**Payashi Garry:** Data acquisition, interpretation of data, critical revision of manuscript, final approval

**Catherine Lamb:** Data acquisition, critical revision of manuscript, final approval

**Michael Kelly:** Data analysis, interpretation of data, critical revision of manuscript, final approval

**Thomas Okell:** Data analysis, interpretation of data, critical revision of manuscript, final approval

**Jon Westbrook:** Study design, critical revision of manuscript, final approval

**Richard D Wise:** Study design, interpretation of data, critical revision of manuscript, final approval

**Gwenaelle Douaud:** Data analysis, interpretation of data, critical revision of manuscript, final approval

**Kyle TS Pattinson:** Study design, interpretation of data, manuscript preparation, final approval

## DISCLOSURE/CONFLICTS OF INTEREST

M.R., M.E., J.W. and K.P. are named as co-inventors on a provisional U.K. patent application titled "Use of cerebral nitric oxide donors in the assessment of the extent of brain dysfunction following injury."

K.P. has acted as a consultant for Nektar Therapeutics. The work for Nektar has no bearing on the contents of this manuscript.

T.W.O. is a co-author of a pending US patent licensed to Siemens Healthcare (Erlangen, Germany) relating to the maximum *a posteriori* VEPCASL processing technique used in this study.

## SUPPLEMENTARY MATERIAL

Supplementary material for this paper is available at:

http://jcbfm.sagepub.com/content/by/supplemental-data

## REFERENCES


1 Berridge MJ, Bootman MD, Roderick HL. Calcium: Calcium signalling: dynamics, homeostasis and remodelling. *Nat Rev Mol Cell Biol* 2003; **4**: 517–529.

2 Pisani A, Calabresi P, Tozzi A, D'Angelo V, Bernardi G. L-type Ca2+ channel blockers attenuate electrical changes and Ca2+ rise induced by oxygen/glucose deprivation in cortical neurons. *Stroke* 1998; **29**: 196–201; discussion 202.

3 Calabresi P, Pisani A, Mercuri NB, Bernardi G. On the mechanisms underlying hypoxia-induced membrane depolarization in striatal neurons. *Brain* 1995; **118 ( Pt 4)**: 1027–1038.

4 Kazda S, Towart R. Nimodipine: a new calcium antagonistic drug with a preferential cerebrovascular action. *Acta Neurochir* 1982; **63**: 259–265.

5 Harris RJ, Branston NM, Symon L, Bayhan M, Watson A. The effects of a calcium antagonist, nimodipine, upon physiological responses of the cerebral vasculature and its possible influence upon focal cerebral ischaemia. *Stroke* 1982; **13**: 759–766.

6 Van Den Kerckhoff W, Drewes LR. Transfer of the Ca-antagonists nifedipine and nimodipine across the blood-brain barrier and their regional distribution in vivo. *Journal of Cerebral Blood Flow & Metabolism* 1985; **5**: 459–460.

7 Rowland MJ, Hadjipavlou G, Kelly M, Westbrook J, Pattinson KTS. Delayed cerebral ischaemia after subarachnoid haemorrhage: looking beyond vasospasm. *Br J Anaesth* 2012; **109**: 315–329.

8 Pisani A, Calabresi P, Tozzi A, D'Angelo V, Bernardi G, Iadecola C. L-Type Ca2+ Channel Blockers Attenuate Electrical Changes and Ca2+ Rise Induced by Oxygen/Glucose Deprivation in Cortical Neurons. *Stroke* 1998; **29**: 196–202.

9 Shoykhet M, Simons DJ, Alexander H, Hosler C, Kochanek PM, Clark RSB. Thalamocortical dysfunction and thalamic injury after asphyxial cardiac arrest in developing rats. *J Neurosci* 2012; **32**: 4972–4981.

10 Canese R, Podo F, Fortuna S, Lorenzini P, Michalek H. Transient global brain ischemia in the rat: spatial distribution, extension, and evolution of lesions evaluated by magnetic resonance imaging. *MAGMA* 1997; **5**: 139–149.

11 Kawai K, Nitecka L, Ruetzler CA, Nagashima G, Joó F, Mies G *et al.* Global cerebral ischemia associated with cardiac arrest in the rat: I. Dynamics of early neuronal changes. *J Cereb Blood Flow Metab* 1992; **12**: 238–249.

12 Böttiger BW, Schmitz B, Wiessner C, Vogel P, Hossmann KA. Neuronal stress response and neuronal cell damage after cardiocirculatory arrest in rats. *J Cereb Blood Flow Metab* 1998; **18**: 1077–1087.

13 Mitchell AS, Dalrymple-Alford JC. Dissociable memory effects after medial thalamus lesions in the rat. *Eur J Neurosci* 2005; **22**: 973–985.

14 Ross DT, Graham DI. Selective loss and selective sparing of neurons in the thalamic

reticular nucleus following human cardiac arrest. *J Cereb Blood Flow Metab* 1993; **13**: 558–567.

15 Ross DT, Graham DI, Adams JH. Selective loss of neurons from the thalamic reticular nucleus following severe human head injury. *J Neurotrauma* 1993; **10**: 151–165.

16 Basso MA, Uhlrich D, Bickford ME. Cortical Function: A View from the Thalamus. *Neuron* 2005; **45**: 485–488.

17 Kallenberg K, Bailey DM, Christ S, Mohr A, Roukens R, Menold E *et al.* Magnetic resonance imaging evidence of cytotoxic cerebral edema in acute mountain sickness. *J Cereb Blood Flow Metab* 2007; **27**: 1064–1071.

18 Rostrup E, Larsson HBW, Born AP, Knudsen GM, Paulson OB. Changes in BOLD and ADC weighted imaging in acute hypoxia during sea-level and altitude adapted states. *NeuroImage* 2005; **28**: 947–955.

19 Schoonman GG, Sándor PS, Nirkko AC, Lange T, Jaermann T, Dydak U *et al.* Hypoxia-induced acute mountain sickness is associated with intracellular cerebral edema: a 3 T magnetic resonance imaging study. *J Cereb Blood Flow Metab* 2008; **28**: 198–206.

20 Palacios EM, Sala-Llonch R, Junque C, Roig T, Tormos JM, Bargallo N *et al.* Resting-State Functional Magnetic Resonance Imaging Activity and Connectivity and Cognitive Outcome in Traumatic Brain Injury. *JAMA Neurol* 2013; **70**: 845–7.

21 Zhang J, Wei L, Hu X, Zhang Y, Zhou D, Li C *et al.* Specific frequency band of amplitude low-frequency fluctuation predicts Parkinson's disease. *Behavioural Brain Research* 2013; **252**: 18–23.

22 Du C, Volkow ND, Koretsky AP, Pan Y. Low-frequency calcium oscillations accompany deoxyhemoglobin oscillations in rat somatosensory cortex. *Proc Natl Acad Sci USA* 2014; **111**: E4677–E4686.

23 Hernández-Hernández R, Coll T, Rachitzky P, Armas-Hernández MJ, Armas-Padilla MC, Velasco M *et al.* Comparison of two nimodipine formulations in healthy volunteers. *J Hum Hypertens* 2002; **16 Suppl 1**: S142–4.

24 Okell TW, Chappell MA, Kelly ME, Jezzard P. Cerebral blood flow quantification using vessel-encoded arterial spin labeling. *J Cereb Blood Flow Metab* 2013; **33**: 1716–1724.

25 Bakker CJ, Hoogeveen RM, Viergever MA. Construction of a protocol for measuring blood flow by two-dimensional phase-contrast MRA. 1999; **9**: 119–127.

26 Smith SM, Jenkinson M, Woolrich MW, Beckmann CF, Behrens TEJ, Johansen-Berg H *et al.* Advances in functional and structural MR image analysis and implementation as FSL. *NeuroImage* 2004; **23 Suppl 1**: S208–19.

27 Douaud G, Smith S, Jenkinson M, Behrens T, Johansen-Berg H, Vickers J *et al.* Anatomically related grey and white matter abnormalities in adolescent-onset schizophrenia. *Brain* 2007; **130**: 2375–2386.

28 Smith SM, Zhang Y, Jenkinson M, Chen J, Matthews PM, Federico A *et al.* Accurate, robust, and automated longitudinal and cross-sectional brain change analysis. *NeuroImage* 2002; **17**: 479–489.

29 Jenkinson M, Smith S. A global optimisation method for robust affine registration of brain images. *Med Image Anal* 2001; **5**: 143–156.

30 Jenkinson M, Bannister P, Brady M, Smith S. Improved optimization for the robust and accurate linear registration and motion correction of brain images. *NeuroImage* 2002; **17**: 825–841.

31 Greve DN, Fischl B. Accurate and robust brain image alignment using boundary-based registration. *NeuroImage* 2009; **48**: 63–72.

32 Chappell MA, Macintosh BJ, Donahue MJ, Günther M, Jezzard P, Woolrich MW. Separation of macrovascular signal in multi-inversion time arterial spin labelling MRI. *Magn Reson Med* 2010; **63**: 1357–1365.

33 Wong EC. Vessel-encoded arterial spin-labeling using pseudocontinuous tagging. *Magn Reson Med* 2007; **58**: 1086–1091.

34 Beckmann CF, DeLuca M, Devlin JT, Smith SM. Investigations into resting-state connectivity using independent component analysis. *Philosophical Transactions of the Royal Society of London B: Biological Sciences* 2005; **360**: 1001–1013.

35 Griffanti L, Douaud G, Bijsterbosch J, Evangelisti S, Alfaro-Almagro F, Glasser MF *et al.* Hand classification of fMRI ICA noise components. *NeuroImage* 2016. doi:10.1016/j.neuroimage.2016.12.036.

36 Salimi-Khorshidi G, Douaud G, Beckmann CF, Glasser MF, Griffanti L, Smith SM. Automatic denoising of functional MRI data: Combining independent component analysis and hierarchical fusion of classifiers. *NeuroImage* 2014; **90**: 449–468.

37 Griffanti L, Salimi-Khorshidi G, Beckmann CF, Auerbach EJ, Douaud G, Sexton CE *et al.* ICA-based artefact removal and accelerated fMRI acquisition for improved resting state network imaging. *NeuroImage* 2014; **95**: 232–247.

38 Brooks JCW, Beckmann CF, Miller KL, Wise RG, Porro CA, Tracey I *et al.* Physiological noise modelling for spinal functional magnetic resonance imaging studies. *NeuroImage* 2008; **39**: 680–692.

39 Harvey AK, Pattinson KTS, Brooks JCW, Mayhew SD, Jenkinson M, Wise RG. Brainstem functional magnetic resonance imaging: Disentangling signal from physiological noise. 2008; **28**: 1337–1344.

40 Faull OK, Jenkinson M, Ezra M, Pattinson K. Conditioned respiratory threat in the subdivisions of the human periaqueductal gray. *Elife* 2016. doi:10.7554/eLife.12047.001.

41 Babadi B, Brown EN. A Review of Multitaper Spectral Analysis. *IEEE Trans Biomed Eng* 2014; **61**: 1555–1564.

42 Winkler AM, Ridgway GR, Webster MA, Smith SM, Nichols TE. Permutation inference for the general linear model. *NeuroImage* 2014; **92**: 381–397.

43 Winkler AM, Ridgway GR, Douaud G, Nichols TE, Smith SM. Faster permutation inference in brain imaging. *NeuroImage* 2016; **141**: 502–516.

44 Smith SM, Nichols TE. Threshold-free cluster enhancement: Addressing problems of smoothing, threshold dependence and localisation in cluster inference. *NeuroImage* 2009; **44**: 83–98.

45 Rupp T, Jubeau M, Lamalle L, Warnking JM, Millet GY, Wuyam B *et al.* Cerebral volumetric changes induced by prolonged hypoxic exposure and whole-body exercise. 2014; **34**: 1802–1809.

46 Lawley JS, Alperin N, Bagci AM, Lee SH, Mullins PG, Oliver SJ *et al.* Normobaric hypoxia and symptoms of acute mountain sickness: Elevated brain volume and intracranial hypertension. *Ann Neurol* 2014; **75**: 890–898.

47 Poulin MJ, Liang PJ, Robbins PA. Dynamics of the cerebral blood flow response to step changes in end-tidal PCO2 and PO2 in humans. *J Appl Physiol* 1996; **81**: 1084–1095.

48 Dubowitz DJ, Dyer EAW, Theilmann RJ, Buxton RB, Hopkins SR. Early brain swelling in acute hypoxia. *J Appl Physiol* 2009; **107**: 244–252.

49 Harper AM, Craigen L, Kazda S. Effect of the calcium antagonist, nimodipine, on cerebral blood flow and metabolism in the primate. *J Cereb Blood Flow Metab* 1981; **1**: 349–356.

50 Haws CW, Gourley JK, Heistad DD. Effects of nimodipine on cerebral blood flow. *J Pharmacol Exp Ther* 1983; **225**: 24–28.

51 Mohamed AA, Mendelow AD, Teasdale GM, Harper AM, McCulloch J. Effect of the calcium antagonist nimodipine on local cerebral blood flow and metabolic coupling. *J Cereb Blood Flow Metab* 1985; **5**: 26–33.

52 Forsman M, Aarseth HP, Nordby HK, Skulberg A, Steen PA. Effects of nimodipine on cerebral blood flow and cerebrospinal fluid pressure after cardiac arrest: correlation with neurologic outcome. *Anesth Analg* 1989; **68**: 436–443.

53 Gaab MR, Haubitz I, Brawanski A, Korn A, Czech T. Acute effects of nimodipine on the cerebral blood flow and intracranial pressure. *Neurochirurgia (Stuttg)* 1985; **28 Suppl 1**: 93–99.

54 Schmidt JF, Waldemar G. Effect of nimodipine on cerebral blood flow in human volunteers. *J Cardiovasc Pharmacol* 1990; **16**: 568–571.

55 Schmidt JF, Waldemar G, Paulson OB. The acute effect of nimodipine on cerebral blood flow, its CO2 reactivity, and cerebral oxygen metabolism in human volunteers. *Acta Neurochir* 1991; **111**: 49–53.

56 Lukyanetz EA, Shkryl VM, Kravchuk OV, Kostyuk PG. Action of hypoxia on different

types of calcium channels in hippocampal neurons. *Biochim Biophys Acta* 2003; **1618**: 33–38.

57 Haile M, Limson F, Gingrich K, Li Y-S, Quartermain D, Blanck T *et al.* Nimodipine prevents transient cognitive dysfunction after moderate hypoxia in adult mice. *J Neurosurg Anesthesiol* 2009; **21**: 140–144.

58 Greiner C, Schmidinger A, Hülsmann S, Moskopp D, Wölfer J, Köhling R *et al.* Acute protective effect of nimodipine and dimethyl sulfoxide against hypoxic and ischemic damage in brain slices. *Brain Res* 2000; **887**: 316–322.

59 Pickard JD, Murray GD, Illingworth R, Shaw MD, Teasdale GM, Foy PM *et al.* Effect of oral nimodipine on cerebral infarction and outcome after subarachnoid haemorrhage: British aneurysm nimodipine trial. *BMJ* 1989; **298**: 636–642.

60 Feigin VL, Rinkel GJ, Algra A, Vermeulen M, van Gijn J. Calcium antagonists in patients with aneurysmal subarachnoid hemorrhage: a systematic review. *Neurology* 1998; **50**: 876–883.

61 Dorhout Mees SM, Rinkel GJE, Feigin VL, Algra A, van den Bergh WM, Vermeulen M *et al.* Calcium antagonists for aneurysmal subarachnoid haemorrhage. *Cochrane Database Syst Rev* 2007; : CD000277.

62 Heffez DS, Passonneau JV. Effect of nimodipine on cerebral metabolism during ischemia and recirculation in the mongolian gerbil. *Journal of Cerebral Blood Flow & …* 1985; **5**: 523–528.

63 Young WL, Chien S. Effect of nimodipine on cerebral blood flow and metabolism in rats during hyperventilation. *Stroke* 1989; **20**: 275–280.

64 McCalden TA, Nath RG, Thiele K. The effects of a calcium antagonist (nimodipine) on basal cerebral blood flow and reactivity to various agonists. *Stroke* 1984; **15**: 527–530.

65 Wang JJ, Chen X, Sah SK, Zeng C, Li YM, Li N *et al.* Amplitude of low-frequency fluctuation (ALFF) and fractional ALFF in migraine patients: a resting-state functional MRI study. *Clinical Radiology* 2016; **71**: 558–564.

66 Wang L, Dai W, Su Y, Wang G, Tan Y, Jin Z *et al.* Amplitude of Low-Frequency Oscillations in First-Episode, Treatment-Naive Patients with Major Depressive Disorder: A Resting-State Functional MRI Study. *PLoS ONE* 2012; **7**: e48658–10.

67 Zhou F, Zhuang Y, Wu L, Zhang N, Zeng X, Gong H *et al.* Increased thalamic intrinsic oscillation amplitude in relapsing–remitting multiple sclerosis associated with the slowed cognitive processing. *Journal of Clinical Imaging* 2014; **38**: 605–610.

68 Jones RA, Müller TB, Haraldseth O, Baptista AM, Oksendal AN. Cerebrovascular changes in rats during ischemia and reperfusion: a comparison of BOLD and first pass bolus tracking techniques. *Magn Reson Med* 1996; **35**: 489–496.

69 Dunn JF, Wadghiri YZ, Meyerand ME. Regional heterogeneity in the brain's response to hypoxia measured using BOLD MR imaging. *Magn Reson Med* 1999; **41**: 850–854.

70 Rostrup E, Larsson HB, Toft PB, Garde K, Henriksen O. Signal changes in gradient echo images of human brain induced by hypo- and hyperoxia. *NMR Biomed* 1995; **8**: 41–47.

## FIGURE LEGENDS

**Figure 1: A**: Study protocol. **B**: Schematic diagram of the breathing apparatus used to maintain hypoxic conditions in both the laboratory and MRI sessions

**Figure 2: A:** $P_{ET}O_2$ values from the laboratory and MRI sessions. **B:** $P_{ET}CO_2$ values from the laboratory and MRI sessions

**Figure 3:** Graphs showing changes in the thalamus for **A:** apparent diffusion coefficient (ADC), **B:** volume and **C:** cerebral blood flow in each of the four experimental conditions

**Figure 4: A**: Regional areas of decreased grey matter apparent diffusion coefficient (ADC) in the hypoxia/placebo condition compared to normoxia/placebo. (In yellow, $p<0.05$ FWE-corrected for multiple comparisons, overlaid onto an MNI152 standard template). **B**: Regional areas of increased grey matter apparent diffusion coefficient (ADC) in the hypoxia/nimodipine condition compared to hypoxia/placebo. (In yellow, $p<0.05$, overlaid onto an MNI152 standard template

**Figure 5: A:** Thalamus and **B:** whole brain grey matter change in ALFF and frequency spectrograms for placebo and nimodipine conditions in normoxia and hypoxia (graphs show mean (solid line) with 95% CI (shaded areas))

**Figure 6:** Correlations for the VBM, DWI, CBF and ALFF analysis between nimodipine levels and effect of nimodipine in hypoxia (Hypoxia/Drug - Hypoxia/Placebo)

## TABLES

**Table 1:** Physiological data, nimodipine levels and phase contrast MRI results for each experimental condition.

| | Normoxia Placebo | Normoxia Nimodipine | Hypoxia Placebo | Hypoxia Nimodipine |
|---|---|---|---|---|
| **SpO2 (%)** | 98 ± 1*** | 98 ± 1 | 85 ± 6*** | 84 ± 7 |
| **HR (bpm)** | 67 ± 2*** | 68 ± 2 | 77 ± 3*** | 79 ± 3 |
| **SBP (mmHg)** | 115 ± 15 | 114 ± 12 | 119 ± 12 | 116 ± 16 |
| **DBP (mmHg)** | 64 ± 6 | 62 ± 7 | 64 ± 6 | 64 ± 6 |
| **MAP (mmHg)** | 80 ± 7 | 79 ± 9 | 82 ± 9 | 82 ± 8 |
| **PETO2 (KPa)** | 14.17 ± 0.12*** | 14.36 ± 0.19 | 7.38 ± 1.18*** | 7.48 ± 1.21 |
| **PETCO2 (KPa)** | 5.35 ± 0.04*** | 5.32 ± 0.08 | 4.80 ± 0.37*** | 4.83 ± 0.29 |
| | | | | |
| **Nimodipine levels (ng/ml)** | 0 | 18.90 ± 20.33 | 0 | 24.07 ± 24.62 |
| | | | | |
| **Phase Contrast Velocities** | | | | |
| **Left carotid (cm/s)** | 30.93***± 5.32 | 28.66 ± 5.92 | 28.37*** ± 4.97 | 27.07 ± 4.46 |
| **Right carotid (cm/s)** | 31.22* ± 4.19 | 31.05 ± 5.67 | 30.38* ± 5.21 | 28.24 ± 5.03 |
| **Left vertebral(cm/s)** | 14.50 ± 3.55 | 14.28 ± 2.39 | 13.87 ± 3.43 | 13.22 ± 3.10 |
| **Right vertebral (cm/s)** | 11.95 ± 3.59 | 11.92 ± 4.43 | 11.96 ± 4.75 | 11.51 ± 2.99 |

Results are presented as mean ± standard deviation (SpO2=oxygen saturations, HR=heart rate, SBP=systolic blood pressure, DBP=diastolic blood pressure, MAP=mean arterial pressure, ETO2=end tidal oxygen, ETCO2=end tidal carbon dioxide).

**SpO2 -** Normoxia/Placebo v Hypoxia Placebo**:** p=< 0.001

**HR -** Normoxia/Placebo v Hypoxia Placebo: p=< 0.001

**ETO2 -** Normoxia/Placebo v Hypoxia Placebo: p=<0.001

**ETCO2 -** Normoxia/Placebo v Hypoxia Placebo: p=<0.001

**Left carotid:** Normoxia/Placebo v Hypoxia Placebo: p=0.001

**Right carotid:** Normoxia/Placebo v Hypoxia Placebo: p=0.0328

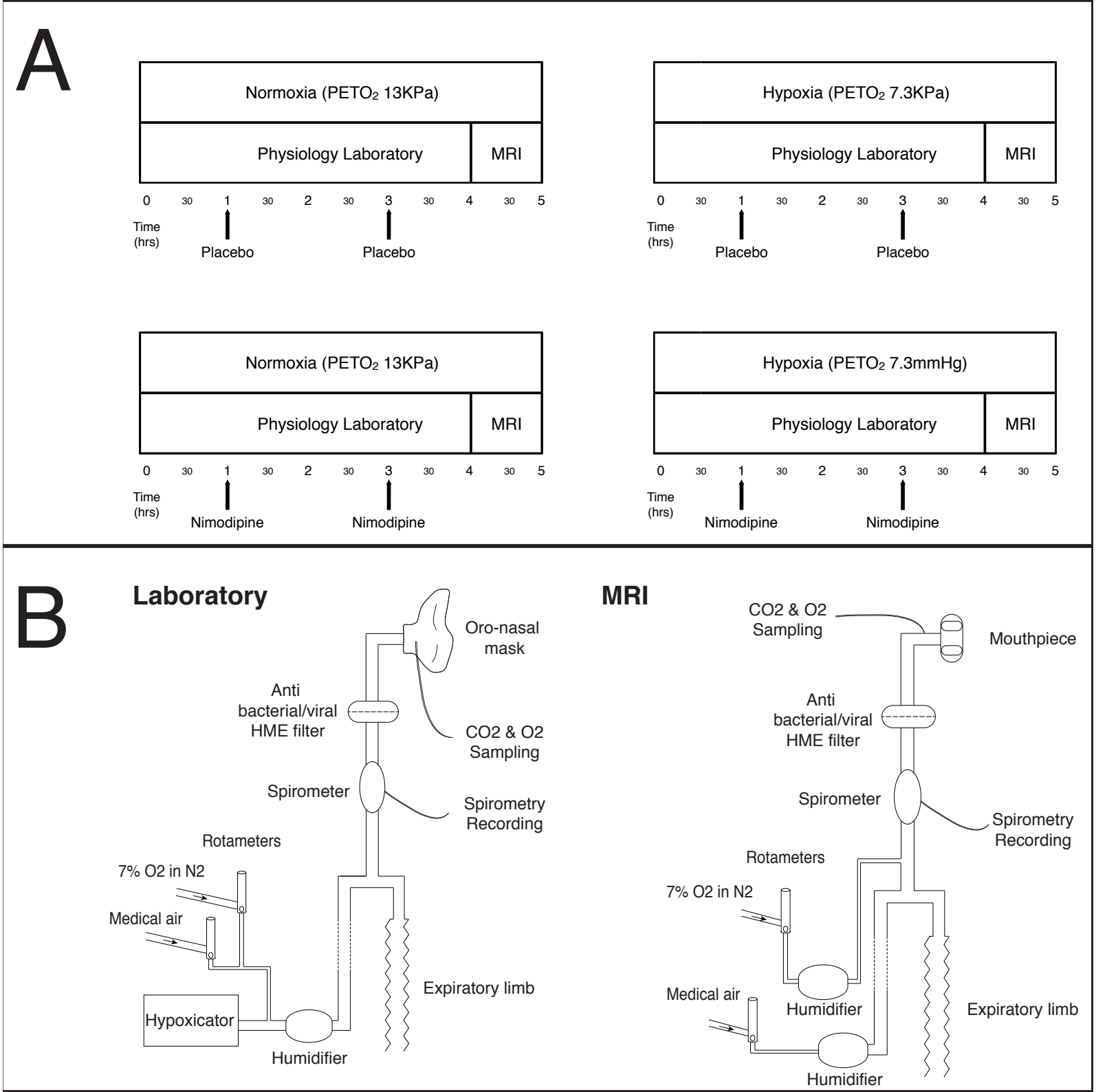
A
Normoxia (PETO2 13KPa)
Physiology Laboratory
MRI
0 30 1 30 2 30 3 30 4 30 5
Time (hrs)
Placebo
Placebo
Hypoxia (PETO2 7.3KPa)
Physiology Laboratory
MRI
0 30 1 30 2 30 3 30 4 30 5
Time (hrs)
Placebo
Placebo
Normoxia (PETO2 13KPa)
Physiology Laboratory
MRI
0 30 1 30 2 30 3 30 4 30 5
Time (hrs)
Nimodipine
Nimodipine
Hypoxia (PETO2 7.3mmHg)
Physiology Laboratory
MRI
0 30 1 30 2 30 3 30 4 30 5
Time (hrs)
Nimodipine
Nimodipine
B
Laboratory
Oro-nasal mask
Anti bacterial/viral HME filter
CO2 & O2 Sampling
Spirometer
Spirometry Recording
Rotameters
7% O2 in N2
Medical air
Hypoxicator
Humidifier
Expiratory limb
MRI
CO2 & O2 Sampling
Mouthpiece
Anti bacterial/viral HME filter
Spirometer
Spirometry Recording
Rotameters
7% O2 in N2
Medical air
Humidifier
Humidifier
Expiratory limb

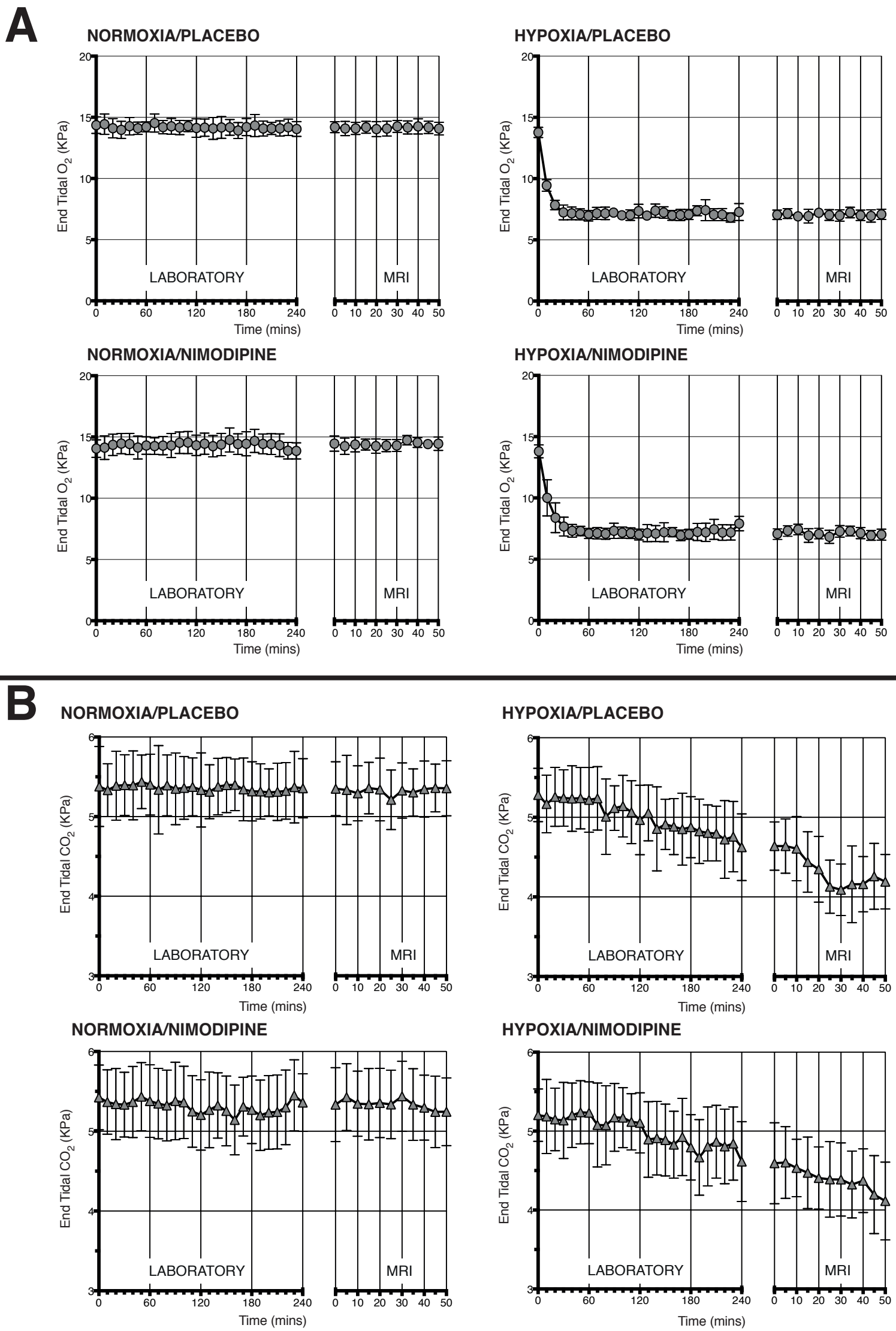
A
NORMOXIA/PLACEBO
HYPOXIA/PLACEBO
NORMOXIA/NIMODIPINE
HYPOXIA/NIMODIPINE
End Tidal $O_2$ (KPa)
LABORATORY
MRI
Time (mins)
B
NORMOXIA/PLACEBO
HYPOXIA/PLACEBO
NORMOXIA/NIMODIPINE
HYPOXIA/NIMODIPINE
End Tidal $CO_2$ (KPa)
LABORATORY
MRI
Time (mins)

# Thalamus

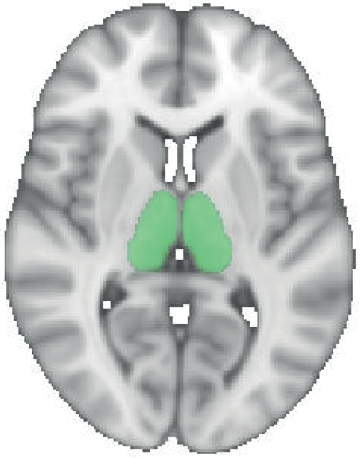

## A: DWI

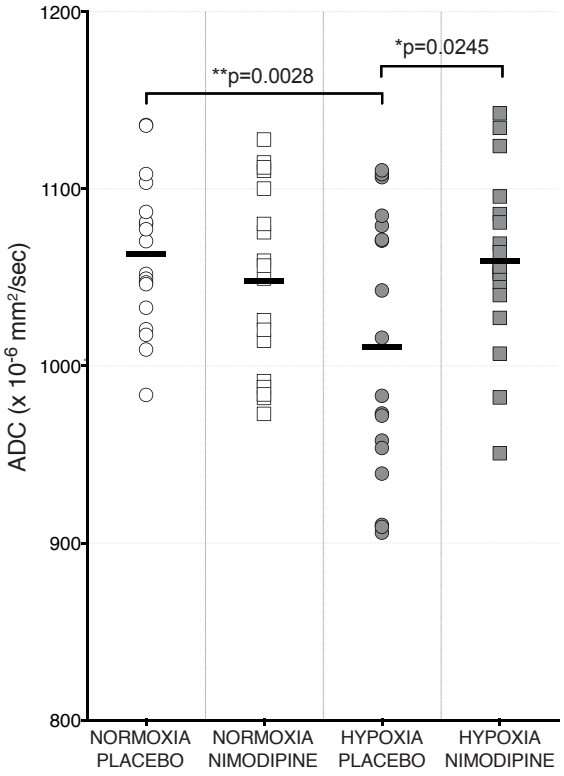


## B: GM volume

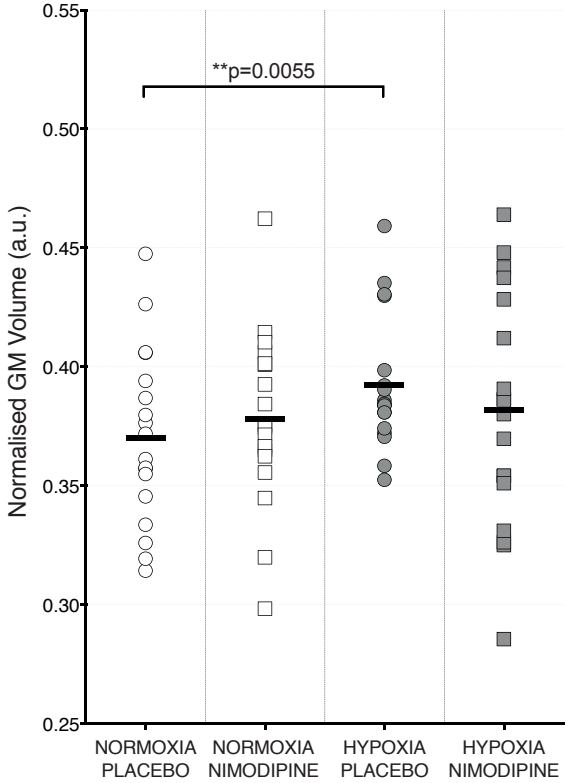


## C: CBF

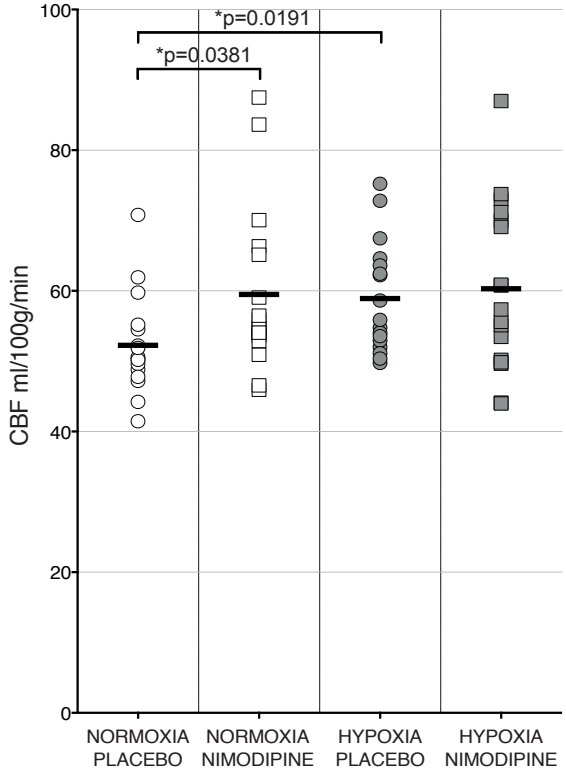

## A: ADC in hypoxia/placebo reduced compared to normoxia/placebo

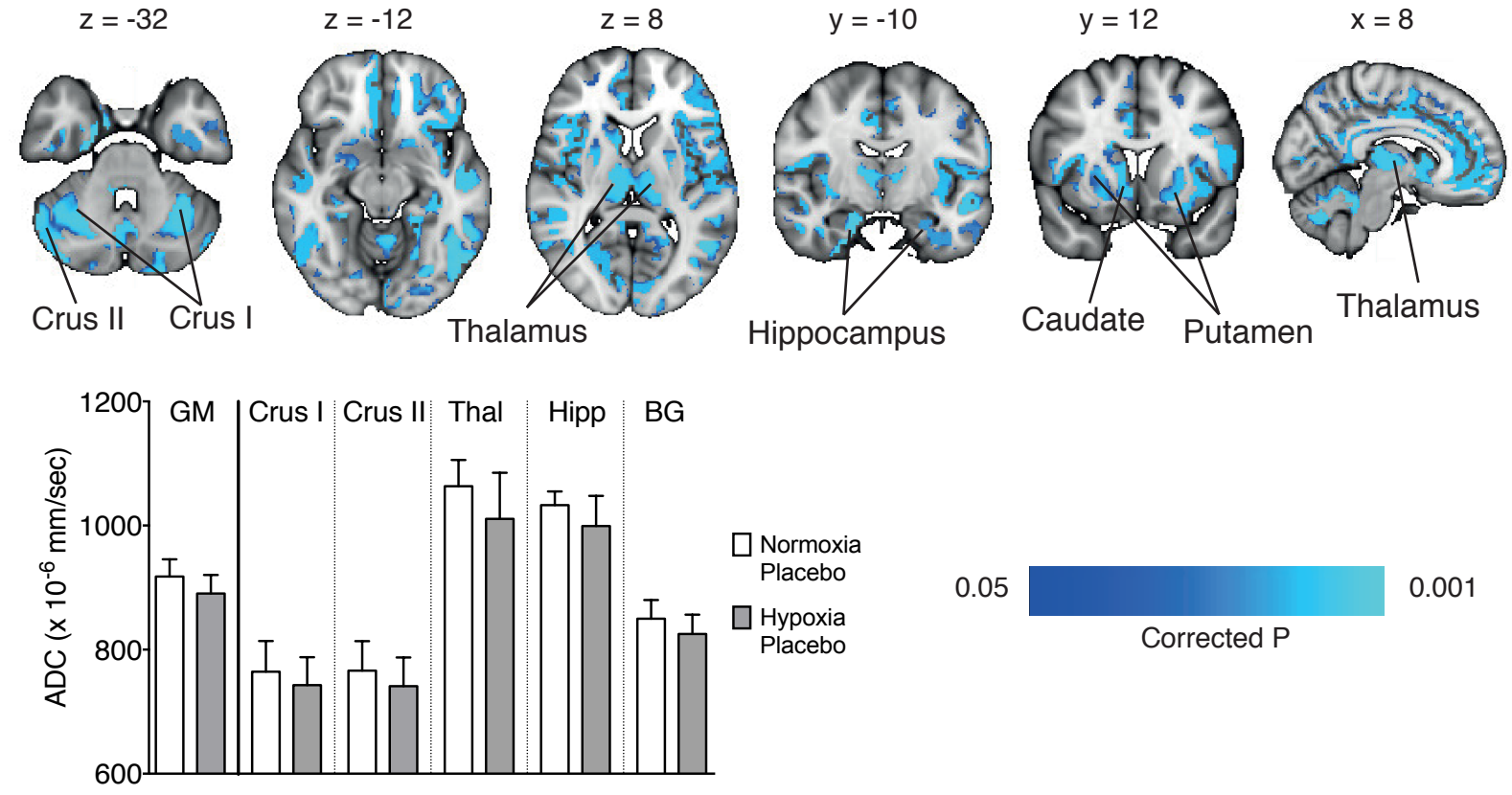


## B: ADC increased in hypoxia/nimodipine compared to hypoxia/placebo

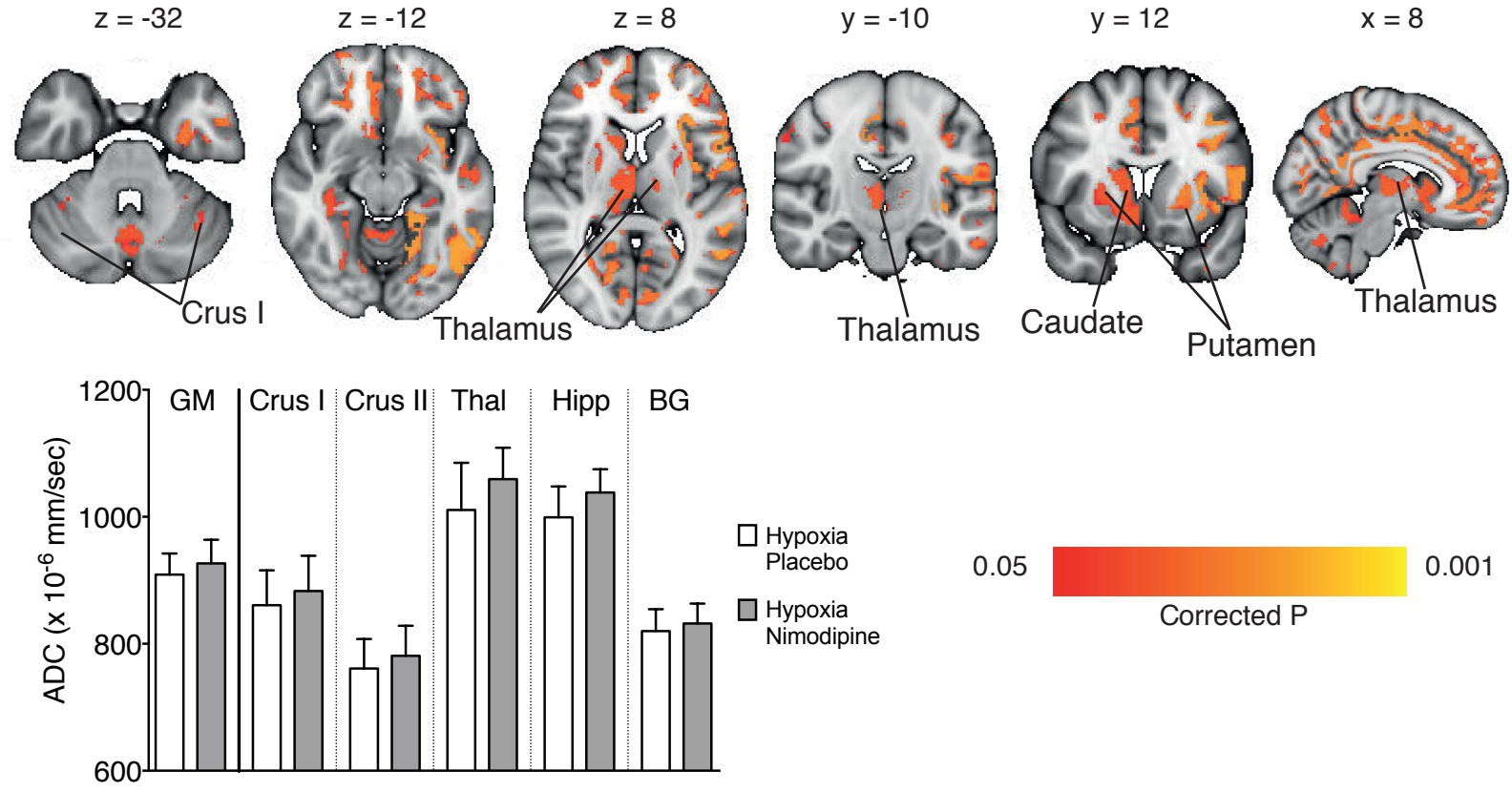

# Amplitude of low frequency BOLD oscillations

## A: Thalamus

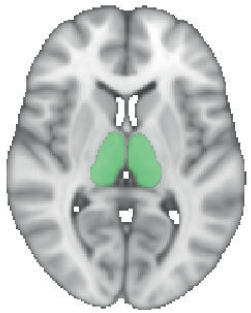

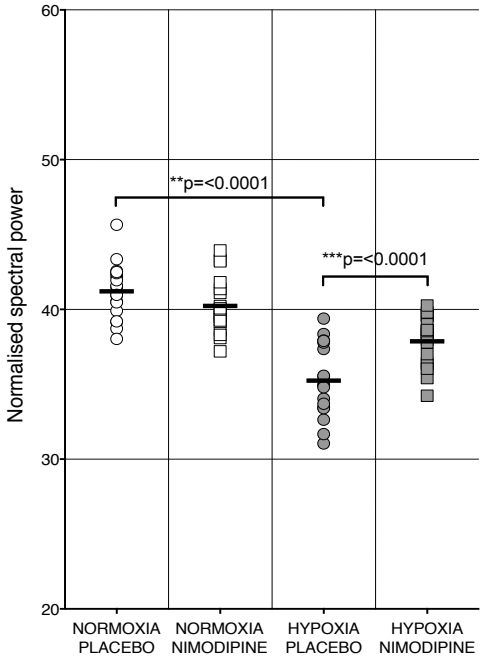


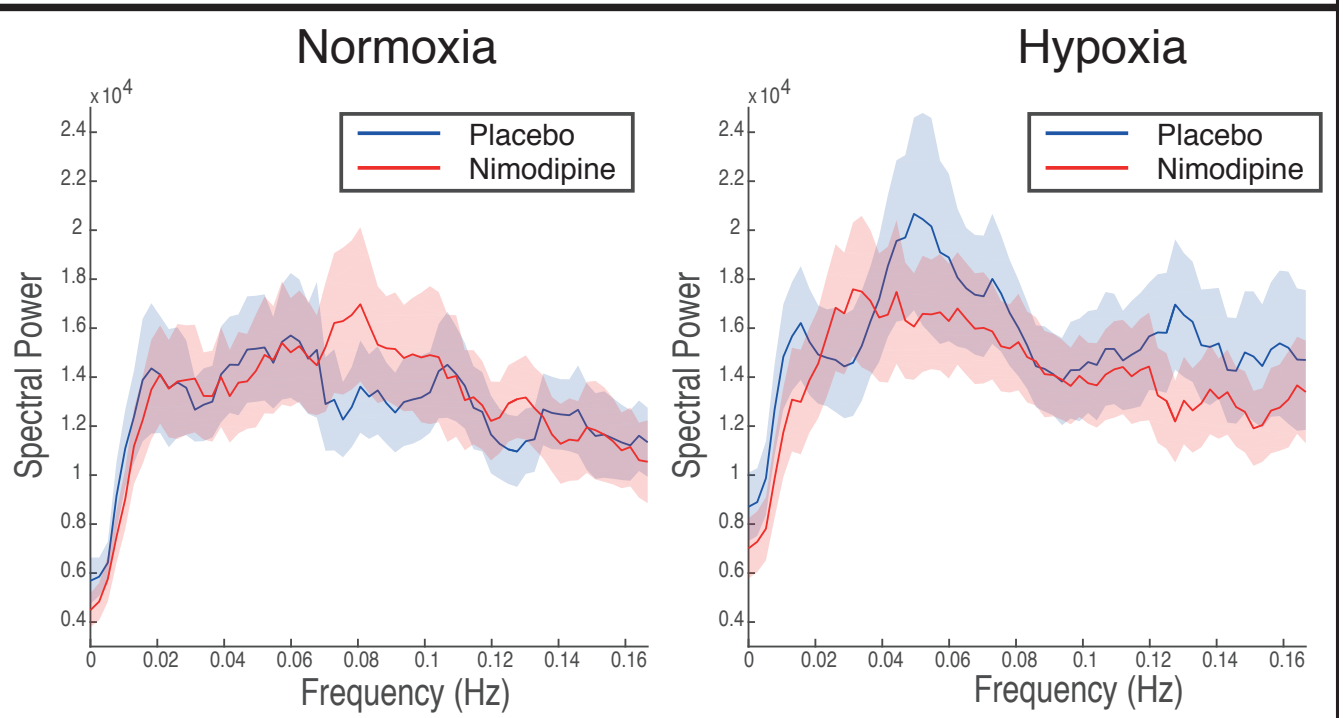


## B: Grey Matter

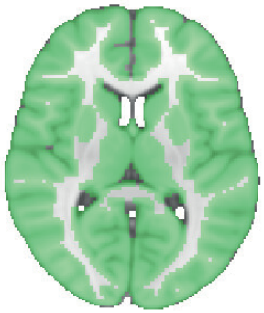

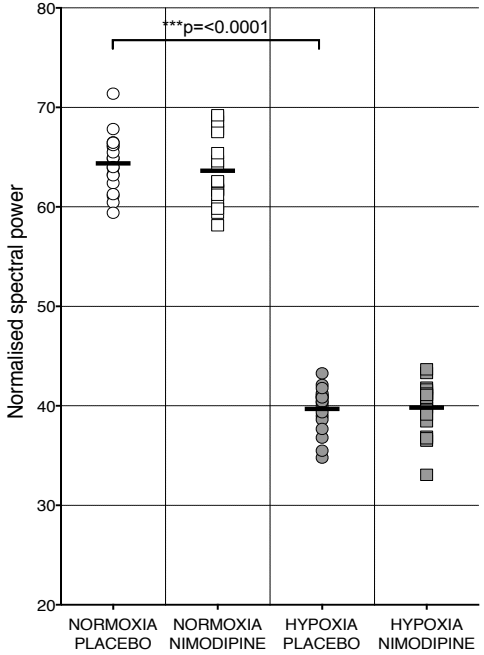


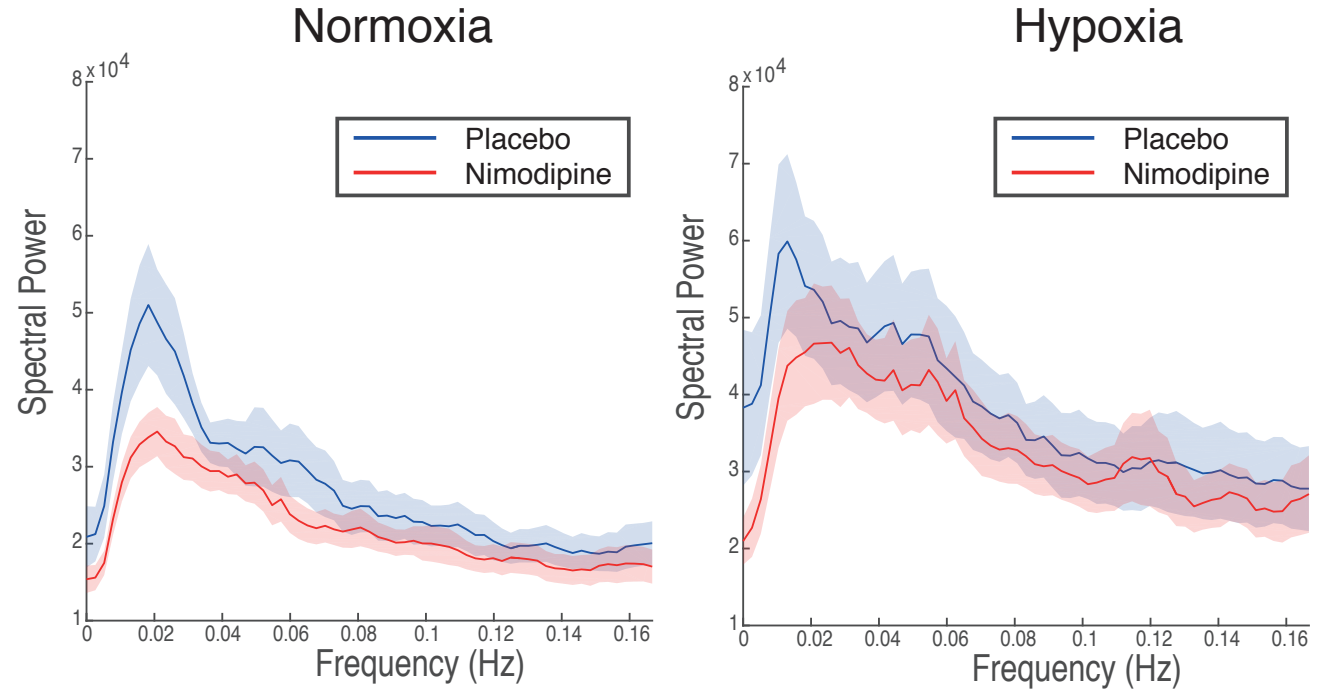

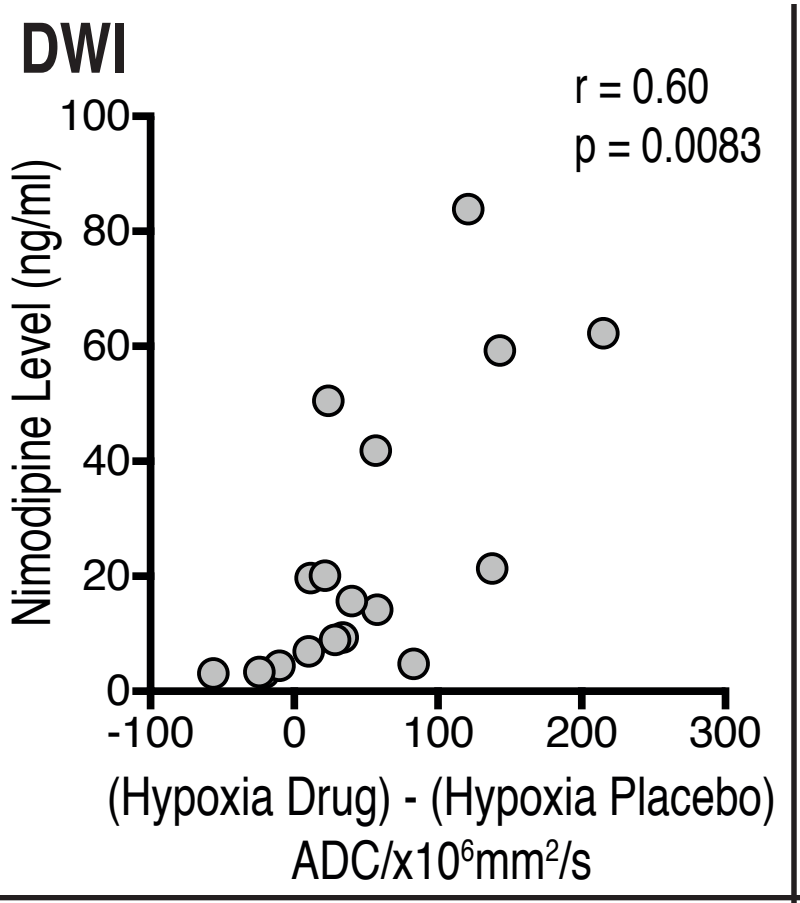
DWI
r = 0.60
p = 0.0083
Nimodipine Level (ng/ml)
100
80
60
40
20
0
-100
0
100
200
300
(Hypoxia Drug) - (Hypoxia Placebo)
ADC/x10⁶mm²/s

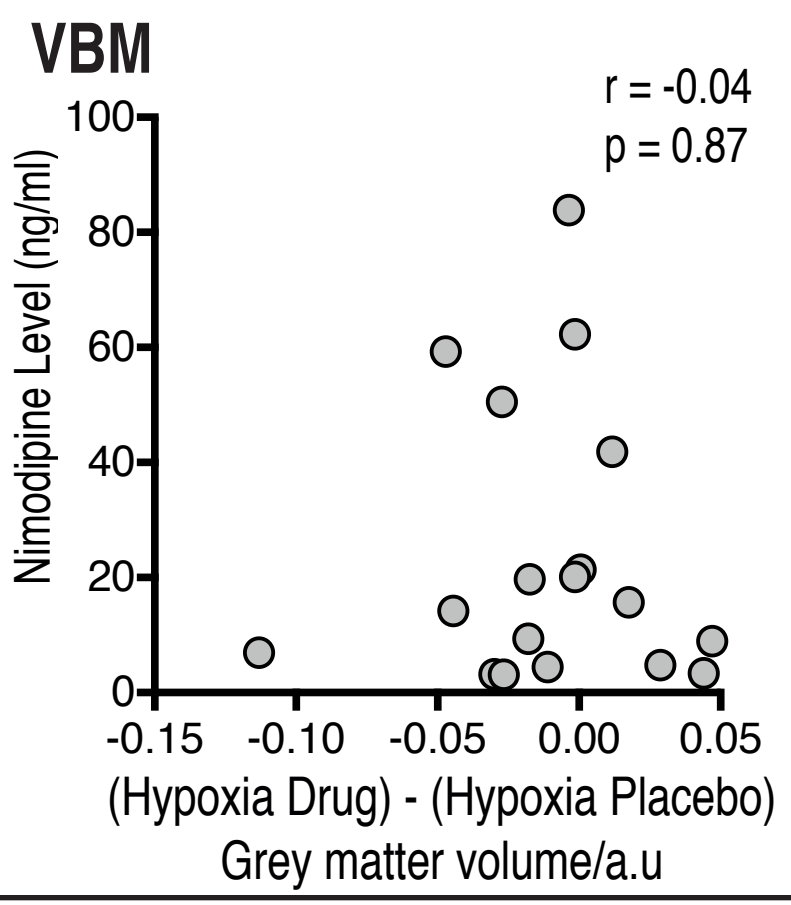
VBM
r = -0.04
p = 0.87
Nimodipine Level (ng/ml)
100
80
60
40
20
0
-0.15
-0.10
-0.05
0.00
0.05
(Hypoxia Drug) - (Hypoxia Placebo)
Grey matter volume/a.u

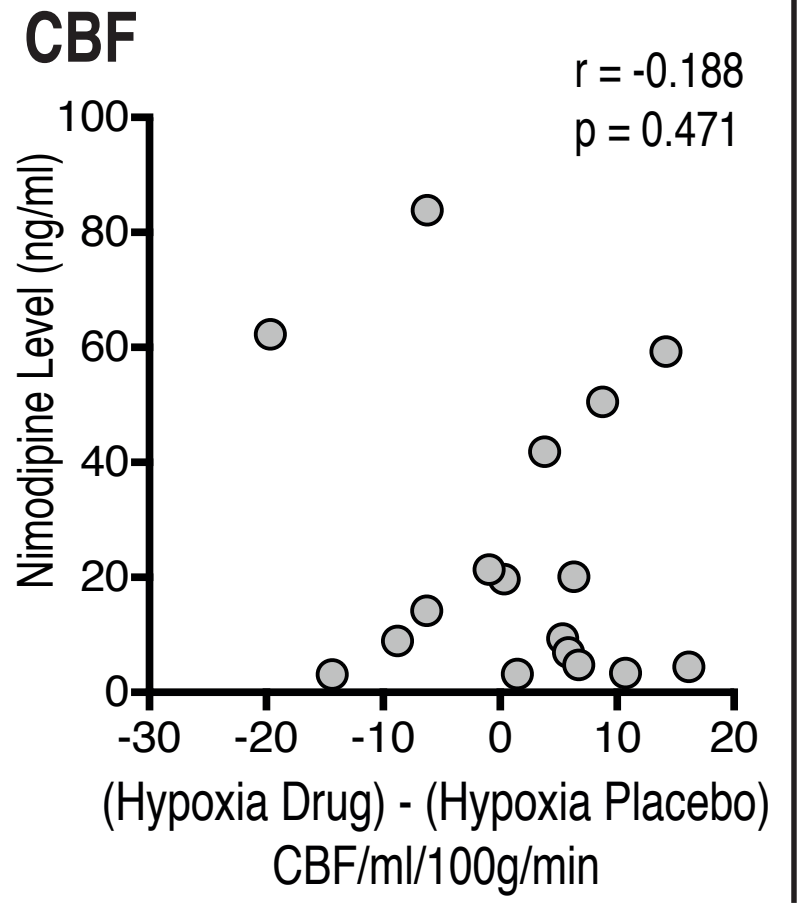
CBF
r = -0.188
p = 0.471
Nimodipine Level (ng/ml)
100
80
60
40
20
0
-30
-20
-10
0
10
20
(Hypoxia Drug) - (Hypoxia Placebo)
CBF/ml/100g/min

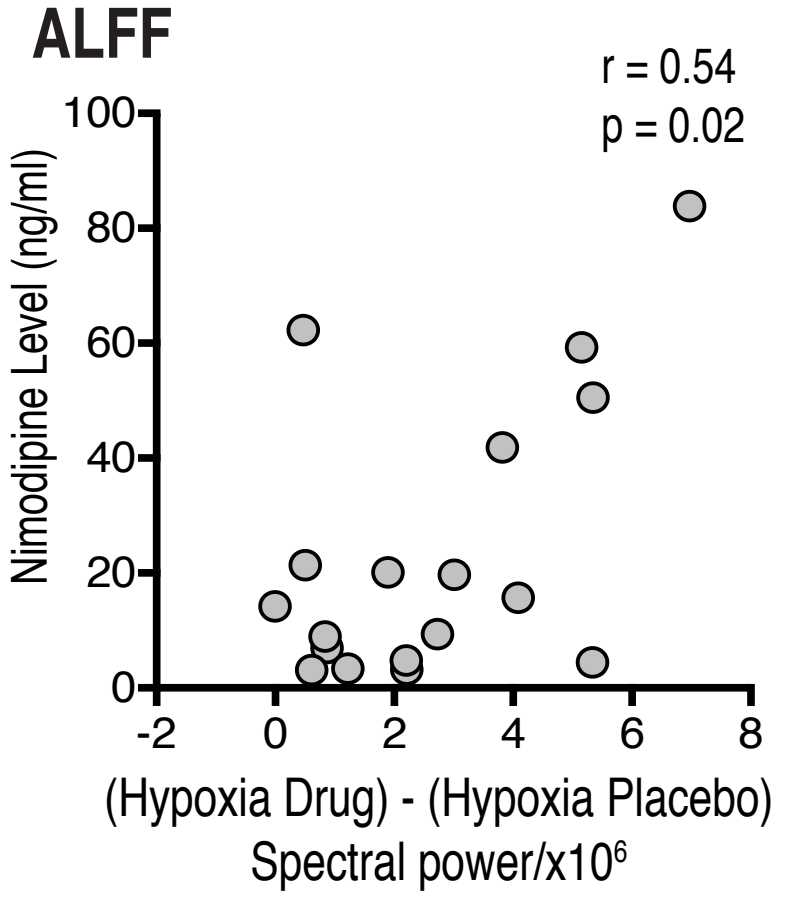
ALFF
r = 0.54
p = 0.02
Nimodipine Level (ng/ml)
100
80
60
40
20
0
-2
0
2
4
6
8
(Hypoxia Drug) - (Hypoxia Placebo)
Spectral power/x10⁶

# SUPPLEMENTARY MATERIAL

**Table S1:** Common local peaks of the significant clusters (P < 0.05 FWE-corrected) showing reduced ADC in hypoxia in contrast to normoxia in the placebo condition. Local maximum t values correspond to Figure 5A.

| **Cortical Region** | **Side** | **MNI Coordinates** | | | **Local maximum t** |
|---|---|---|---|---|---|
| GM Visual Cortex V5 | Lt | -52 | -66 | -6 | 6.6 |
| GM Visual Cortex V2 | Lt | -4 | -70 | 30 | 3.98 |
| GM Visual Cortex V1 | Rt | 18 | -68 | 8 | 4.94 |
| Auditory cortex | Rt | 48 | -16 | 8 | 4.78 |
| Parahippocampal gyrus | Rt | 20 | -10 | -30 | 5.66 |
| Entorhinal cortex | Rt | 22 | -6 | -36 | 5.47 |
| Superior temporal gyrus | Rt | 50 | -22 | 0 | 5.93 |
| Middle temporal gyrus | Rt | 56 | -20 | -18 | 6.3 |
| Inferior temporal gyrus | Rt | 54 | -52 | -20 | 5.22 |
| Temporal fusiform cortex | Lt | -32 | -24 | -24 | 4.26 |
| Frontal operculum cortex | Rt | -42 | 28 | 2 | 5.63 |
| Central operculum cortex | Rt | 56 | -8 | 14 | 4.0 |
| Frontal pole | Lt | -46 | 48 | 0 | 4.42 |
| Frontal medial cortex | Lt | -12 | 38 | -10 | 3.37 |
| Frontal orbital cortex | Lt | -48 | 28 | -14 | 3.03 |
| Inferior frontal gyrus | Lt | -54 | 14 | 16 | 5.18 |
| Precentral gyrus | Lt | -12 | -28 | 44 | 5.12 |
| Postcentral gyrus | Lt | -62 | -16 | 24 | 3.91 |
| Paracingulate gyrus | Rt | 8 | 48 | -2 | 4.85 |
| Cingulate gyrus | Rt | 4 | -48 | 20 | 4.44 |
| Superior parietal lobule | Lt | -2 | -38 | 58 | 3.52 |
| Inferior parietal lobule | Rt | 50 | -34 | 30 | 4.95 |
| Inferior parietal lobule (angular gyrus) | Rt | 52 | -52 | 18 | 4.3 |
| Insular cortex | Lt | -42 | 4 | -4 | 4.63 |
| Precuneus cortex | Rt | 22 | -56 | 20 | 4.01 |
| Thalamus | Rt | 12 | -18 | 8 | 5.0 |
| | Lt | -16 | -20 | 12 | 4.25 |
| Putamen | Rt | 32 | -16 | -2 | 4.74 |
| Putamen | Lt | -28 | -18 | 6 | 3.25 |
| Caudate | Rt | 10 | 6 | 4 | 3.13 |
| Hippocampus | Lt | -22 | -38 | 0 | 4.76 |
| Amygdala | Lt | -26 | -6 | -20 | 3.4 |
| | | | | | |
| **Cerebellum** | | | | | |
| Cerebellum (VIIb) | Lt | -22 | -72 | -46 | 6.15 |
| Cerebellum (VIIb) | Rt | 16 | -74 | -44 | 3.29 |
| Cerebellum (Vermis VIIa) | Rt | 6 | -68 | -38 | 6.4 |
| Cerebellum (VI) | Lt | -12 | -74 | -20 | 6.4 |
| Cerebellum (VI) | Rt | 14 | -64 | -22 | 3.9 |
| Cerebellum (Crus II) | Lt | -36 | -62 | -42 | 5.16 |
| Cerebellum (Crus II) | Rt | 48 | -64 | -48 | 4.12 |
| Cerebellum (Crus I) | Rt | 40 | -66 | -28 | 4.95 |
| Cerebellum (Crus I) | Lt | -38 | -56 | -28 | 4.83 |
| Cerebellum (I-IV) | Rt | 8 | -50 | -20 | 4.39 |
| Cerebellum (I-IV) | Lt | -4 | -54 | -18 | 3.94 |

**Table S2:** Common local peaks of the significant clusters (P < 0.05 FWE-corrected) showing increased ADC with nimodipine in hypoxia in contrast to placebo. Local maximum t values correspond to Fig. 5B. GM = Grey matter

| **Cortical Region** | **Side** | **MNI Coordinates** | | | **Local maximum t** |
|---|---|---|---|---|---|
| GM Visual Cortex V2 | Lt | -18 | -54 | -6 | 3.05 |
| GM Visual Cortex V1 (BA 17) | Lt | -2 | -64 | 4 | 3.18 |
| Superior parietal lobule | Lt | -26 | -66 | 48 | 4.04 |
| Supramarginal gyrus | Lt | -56 | -48 | 24 | 4.07 |
| Inferior parietal lobule | Rt | 58 | -36 | 52 | 6.3 |
| Lateral occipital cortex | Lt | -42 | -74 | -6 | 5.33 |
| Frontal pole | Rt | 24 | 56 | -6 | 4.02 |
| Frontal pole | Lt | -38 | 50 | -2 | 4.08 |
| Premotor cortex (BA 6) | Rt | 8 | 2 | 48 | 3.36 |
| Entorhinal cortex | Lt | -30 | -8 | -42 | 5.76 |
| Precentral gyrus (BA 44) | Lt | -52 | 6 | 8 | 3.45 |
| Postcentral gyrus | Lt | -68 | -14 | 14 | 6.11 |
| Postcentral gyrus | Rt | 66 | -8 | 32 | 3.06 |
| Superior frontal gyrus (BA 1) | Lt | -20 | 36 | 36 | 4.21 |
| Middle frontal gyrus (BA44) | Rt | 26 | 32 | 38 | 4.77 |
| Superior temporal gyrus | Lt | -56 | -38 | 8 | 3.34 |
| Middle temporal gyrus | Lt | -58 | -46 | -4 | 4.03 |
| Middle temporal gyrus | Lt | -44 | -28 | -26 | 3.21 |
| Temporal pole | Lt | -34 | 6 | -38 | 4.22 |
| Cingulate gyrus | Rt | 10 | -50 | 24 | 3.95 |
| Paracingulate gyrus | Rt | 10 | 46 | -4 | 3.8 |
| Hippocampus | Rt | 22 | -8 | -24 | 4.19 |
| Parahippocampal gyrus | Lt | -24 | -40 | -16 | 3.31 |
| Parahippocampal gyrus | Rt | 34 | -34 | -14 | 3.36 |
| Thalamus | Rt | 8 | -16 | 0 | 3.59 |
| Hippocampus | Lt | -18 | -38 | 2 | 3.94 |
| Putamen | Lt | -30 | 0 | -6 | 3.47 |
| Putamen | Rt | 24 | 8 | 4 | 4.15 |
| Subcallosal cortex | Rt | 12 | 16 | -14 | 3.08 |
| Insular cortex | Lt | -42 | -12 | 2 | 3.04 |
| | | | | | |
| **Cerebellum** | | | | | |
| Cerebellum (Crus II) | Lt | -18 | -78 | -48 | 4.08 |
| Cerebellum (VI) | Lt | -22 | -72 | -22 | 3.68 |
| Cerebellum (VI) | Rt | 18 | -62 | -24 | 4.21 |
| Cerebellum (V) | Rt | 16 | -50 | -24 | 4.11 |
| Cerebellum (I-IV) | Lt | -2 | -52 | -14 | 3.28 |

**Figure S3:** ALFF results in the thalamus for each experimental condition following supplementary data denoising with FIX and RETROICOR

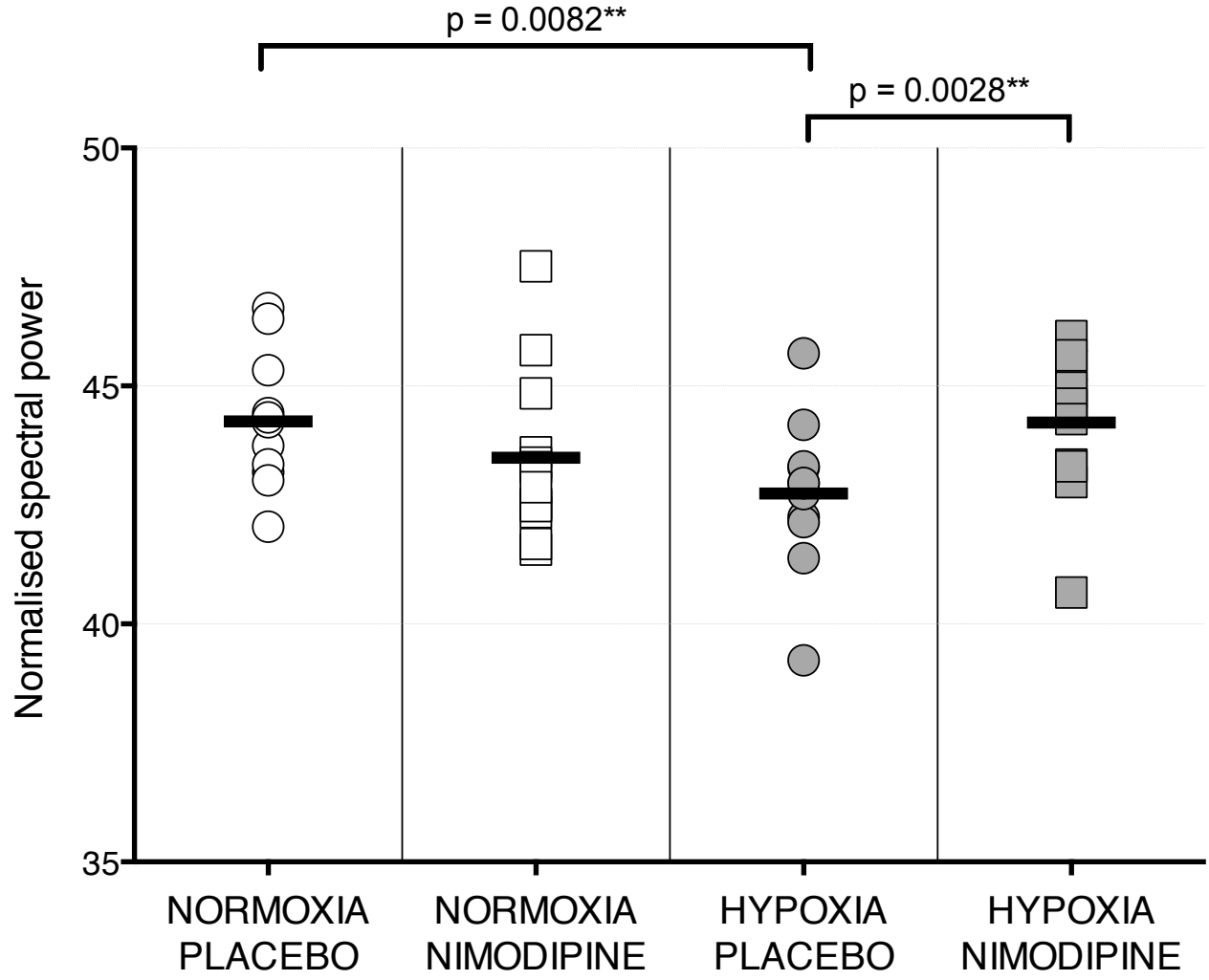

**Figure S4:** Graphs of spectral power for each experimental condition for the thalamus ROI following denoising with both ICA and RETROICOR

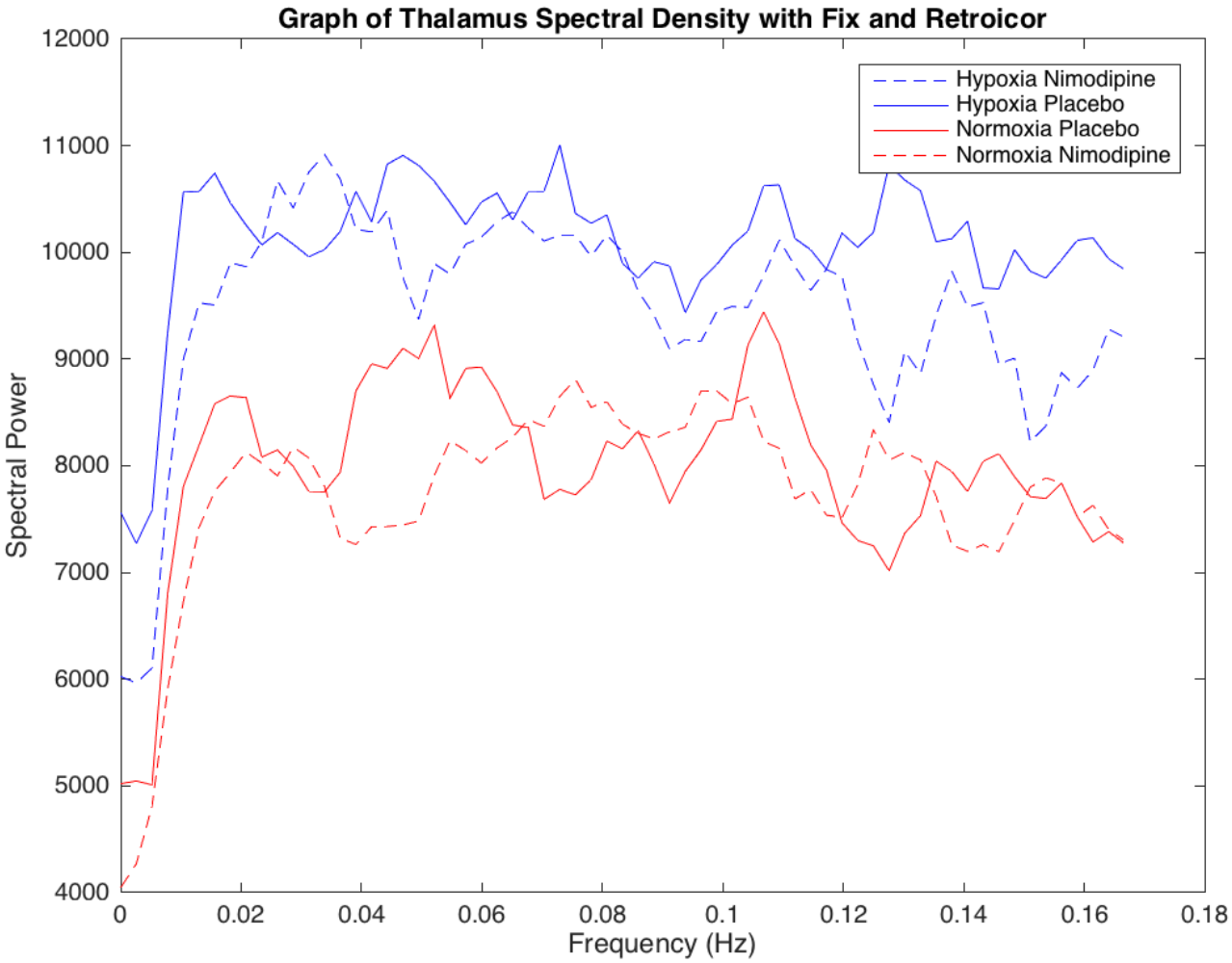

**Figure S5:** Graphs of spectral power for each experimental condition for whole brain grey matter following denoising with both ICA and RETROICOR

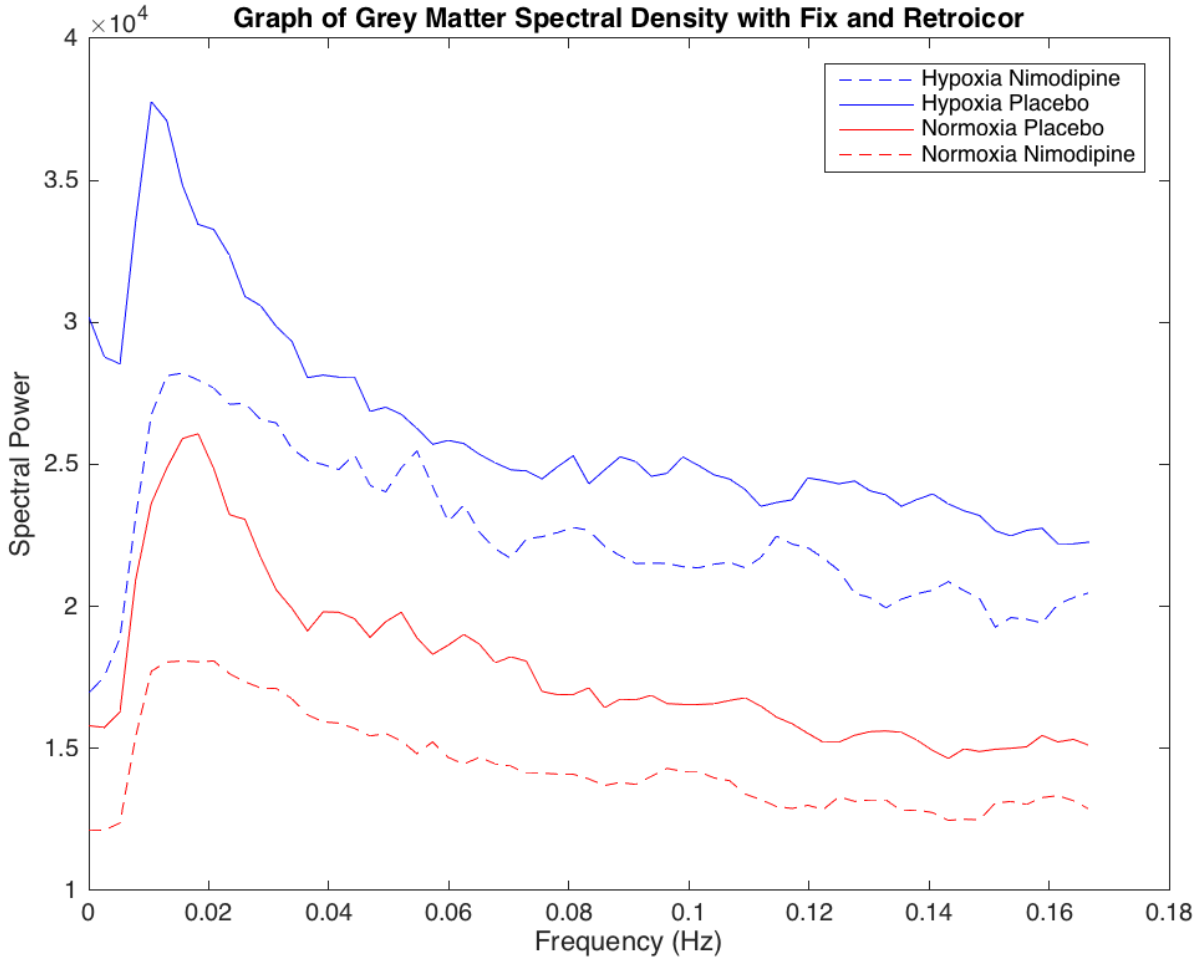

**Figure S6:** Graphs of spectral power for each experimental condition for the thalamus ROI with no data denoising